Examination of Brown Carbon Absorption from Wildfires in the Western U.S. During the WE-CAN Study

Amy P. Sullivan[1], Rudra P. Pokhrel[2,*], Yingjie Shen[2], Shane M. Murphy[2], Darin W. Toohey[3], Teresa Campos[4], Jakob Lindaas[1], Emily V. Fischer[1], and Jeffrey L. Collett, Jr.[1]

[1]Colorado State University, Department of Atmospheric Science, Fort Collins, Colorado 80523
[2]University of Wyoming, Department of Atmospheric Science, Laramie, WY 82071
[3]University of Colorado – Boulder, Department of Atmospheric and Oceanic Sciences, Boulder, CO 80309
[4]National Center for Atmospheric Research, Atmospheric Chemistry Division, Boulder, CO
*now at Cooperative Institute for Research in Environmental Sciences, University of Colorado, Boulder, CO 80309 and NOAA Chemical Science Laboratory, Boulder, CO 80305

Corresponding author: Amy P. Sullivan, sullivan@atmos.colostate.edu

Abstract

Light absorbing organic carbon, or brown carbon (BrC), can be a significant contributor to the visible light absorption budget. However, the sources of BrC and the contributions of BrC to light absorption are not well understood. Biomass burning is thought to be a major source of BrC. Therefore, as part of the WE-CAN (Western Wildfire Experiment for Cloud Chemistry, Aerosol Absorption and Nitrogen) Study BrC absorption data was collected aboard the NSF/NCAR C-130 aircraft as it intercepted smoke from wildfires in the Western U.S. in July-August 2018. BrC absorption measurements were obtained in near real-time using two techniques. The first coupled a Particle-into-Liquid Sampler (PILS) with a Liquid Waveguide Capillary Cell and a Total Organic Carbon analyzer for measurements of water-soluble BrC absorption and WSOC (water-soluble organic carbon). The second employed a custom-built Photoacoustic Aerosol Absorption Spectrometer (PAS) to measure total absorption at 405 and 660 nm. The PAS BrC absorption at 405 nm (PAS total Abs 405 BrC) was calculated by assuming the absorption determined by the PAS at 660 nm was equivalent to the black carbon (BC) absorption and the BC aerosol absorption Ångström exponent was 1. Data from the PILS and PAS were combined to investigate the water-soluble vs. total BrC absorption at 405 nm in the various wildfire plumes sampled during WE-CAN. WSOC, PILS water-soluble Abs 405, and PAS total Abs 405 tracked each other in and out of the smoke plumes. BrC absorption was correlated with WSOC (R^2 value for PAS = 0.42 and PILS = 0.60) and CO (carbon monoxide) (R^2 value for PAS = 0.76 and PILS = 0.55) for all wildfires sampled. The PILS water-soluble Abs 405 was corrected for the non-water-soluble fraction of the aerosol using the calculated UHSAS (Ultra-High-Sensitivity Aerosol Spectrometer) aerosol mass. The corrected PILS water-soluble Abs 405 showed good closure with the PAS total Abs 405 BrC with a factor of ~1.5 to 2 difference. This difference was explained by particle vs. bulk solution absorption measured by the PAS vs. PILS, respectively, and confirmed by Mie Theory calculations. During WE-CAN, ~45% (ranging from 31% to 65%) of the BrC absorption was observed to be due to water-soluble species. The ratio of BrC absorption to WSOC or ΔCO showed no clear dependence on fire dynamics or the time since emission over 9 h.

1. Introduction

Organic compounds can comprise a large fraction of PM (particulate matter) mass [*Kanakidou et al.*, 2005; *Zhang et al.*, 2007]. Organic carbon can be directly emitted or formed in the atmosphere from a variety of sources. This leads to organic aerosol particles composed of a number of compounds that range from insoluble to highly water-soluble and that can scatter or absorb light [*Jacobson et al.*, 2000; *Saxena and Hildemann*, 1996, and references therein].

The portion of organic carbon that is light-absorbing has been referred to as brown carbon (BrC) due to its yellow or brown color when concentrated, and it is likely to be a significant contributor to the visible light-absorption budget [*Andreae and Gelencsér*, 2006]. Recent modeling studies have predicted a non-negligible effect on the Earth's radiation balance from BrC [*Feng et al.*, 2013; *Zhang et al.*, 2017; *Zhang et al.*, 2020]. Global measurements have shown that BrC can contribute up to 48% of the overall warming effect by absorbing carbonaceous aerosols [*Zeng et al.*, 2020]. BrC may also suppress photolysis rates of some chemical reactions, including decreasing surface ozone concentrations in certain locations, due to its ability to absorb at ultraviolet wavelengths [*Jo et al.*, 2016]. Some portion of BrC is likely composed of toxins, such as nitro- and oxy-aromatic species, suggesting BrC could also have health impacts [*Desyaterik et al.*, 2013; *Verma et al.*, 2015; *Zhang et al.*, 2013]. BrC itself is thought to have both primary and secondary sources. Particles from biomass burning or incomplete combustion of fossil fuels generally contain significant amounts of BrC (e.g., [*Chakrabarty et al.*, 2010; *Hoffer et al.*, 2006; *Kirchstetter et al.*, 2004; *Kirchstetter and Thatcher*, 2012; *Lack et al.*, 2012; *Lukács et al.*, 2007]). Laboratory studies have observed production of BrC from a number of formation processes. This has included heterogenous reactions of isoprene on acidic aerosol particles, a variety of aqueous-phase reactions, and reactions of organic compounds in acidic solutions (e.g., [*Hoffer et al.*, 2006; *Limbeck et al.*, 2013; *Sareen et al.*, 2010; *Updyke et al.*, 2012]). However, there is still limited information on the contribution of BrC to total light absorption and the sources of BrC as there are few ambient measurements.

Total absorption measurements (black carbon (BC) + BrC) at multiple wavelengths can be used to determined BrC absorption due to the strong wavelength dependence of BrC. This requires the assumptions that: (1) the absorption Ångström exponent (AAE) for BC is known, (2) AAE is constant with wavelength, and (3) BrC does not absorb at longer wavelengths. The AAE for BC is well constrained at 1 in the visible and near-infrared wavelengths [*Moosmüller et al.*, 2009]. The BrC absorption at other wavelengths is then found by difference from the extrapolated BC AAE [*Lack and Langridge*, 2013; *Mohr et al.*, 2013]. This approach can be applied to any technique that measures absorption at multiple wavelengths, including photoacoustic spectroscopy (PAS).

BrC can also be quantified by isolating the BrC chromophores by extraction of particles in solvents, such as water or methanol, in order to separate them from the insoluble BC and then measuring the light absorption of the soluble organic chromophores [*Hecobian et al.*, 2010]. This is the only direct method to separate and quantify BrC as the light absorption from liquid extracts does not suffer from interferences by BC as they can be isolated by dissolution. A spectrophotometer with an UV/Vis (ultraviolet/visible) light source can provide high spectral resolution over a wide wavelength range from 200 to 800 nm. In addition, when coupled with a long-path liquid waveguide capillary absorption cell (LWCC), it also provides a highly sensitive measurement. This technique can be used off-line with filters or on-line with an aerosol

138   collection device such as Particle-into-Liquid Sampler (PILS) (e.g., [*Hecobian et al.*, 2010; *Liu*
139   *et al.*, 2013, 2014, 2015; *Zhang et al.*, 2011, 2013].
140   Here we report BrC absorption data from a PAS and PILS-LWCC-TOC system to
141   compare total vs. water-soluble BrC absorption in wildfire smoke. Data are from smoke plume
142   penetrations during the Western Wildfire Experiment for Cloud Chemistry, Aerosol Absorption
143   and Nitrogen (WE-CAN), an aircraft-based study focused on investigating the chemistry and
144   transformation of emissions from wildfires in the western U.S. We examine the relationship
145   between the BrC absorption and species known to be from biomass burning. We discuss how
146   parameters such as aging and fire dynamics might influence BrC absorption from wildfires.
147
148   **2. Methods**
149   **2.1. The Airborne Mission**
150   The WE-CAN Campaign was a multi-investigator study conducted aboard the National
151   Science Foundation/National Center for Atmospheric Research (NSF/NCAR) C-130 aircraft.
152   The C-130 was operated out of Boise, ID from Jul. 20 to Aug. 31, 2018. A suite of instruments
153   was deployed for measurements of aerosol and trace gas composition. A total of 16 research
154   flights sampled wildfire smoke over the western U.S. to characterize emissions, mixing,
155   chemical transformations, and transport. Figure 1 presents a map of the flight transects and
156   locations of the wildfires sampled. (We exclude Flight RF14, which was conducted off the coast
157   of CA to sample a stratus deck impacted by smoke, and Flight RF16, which consisted of an
158   intercomparison performed near Boise between WE-CAN and BB-FLUX (Biomass Burning
159   Flux Measurements of Trace Gases and Aerosols) common measurements.) More information
160   on each wildfire including the type of fuel consumed is available in the WE-CAN Field Catalog
161   (catalog.eol.ucar.edu/we-can). WE-CAN sampled both fresh and aged (for Flights RF05 and
162   RF08 along with parts of Flights RF07 and RF13) emissions from smoke for wildfires burning in
163   CA, OR, WA, ID, MT, UT, and NV. The general sampling strategy was to circle the wildfire at
164   the source and then follow the smoke downwind using a multiple transect search and rescue
165   pattern to examine smoke evolution. Typically, wildfire smoke plumes were sampled in the free
166   troposphere between 3-5 km during early afternoon to evening periods (20:00 to 02:00 UTC or
167   14:00 to 20:00 LT). Flight RF08 and part of Flight RF07 were exceptions as the aircraft sampled
168   the boundary layer (below 2 km) over the Central Valley of CA.
169
170   **2.2. Particle Collection**
171   During WE-CAN, we deployed two Particle-into-Liquid Sampler (PILS) systems. A
172   PILS is an aerosol collection device that continuously collects ambient particles into purified
173   water [*Orsini et al.*, 2003]. After particles are grown inside the body of the PILS by water
174   condensation in a supersaturated water vapor environment, formed through mixing the ambient
175   air sample with saturated air (100% relative humidity) at higher temperature, the particles are
176   collected by an impactor. The impactor plate is continually washed off by a flow of liquid
177   passed over the impactor, providing a liquid sample containing dissolved aerosol particles which
178   can be analyzed by various methods. Each PILS system sampled from their own Submicron
179   Aerosol Inlet (SMAI) [*Craig et al.*, 2013a, 2013b, 2014; *Moharreri et al.*, 2014] mounted to the
180   belly of the NSF/NCAR C-130. The size-cut for each PILS was provided by a nonrotating
181   MOUDI impactor stage with a 50% transmission efficiency of 1 μm aerodynamic diameter (i.e.,
182   PM_1) at 1 atmosphere ambient pressure [*Marple et al.*, 1991]. The flowrate of 15 LPM was
183   sampled by each PILS through the inlet and MOUDI stage. An activated carbon parallel plate
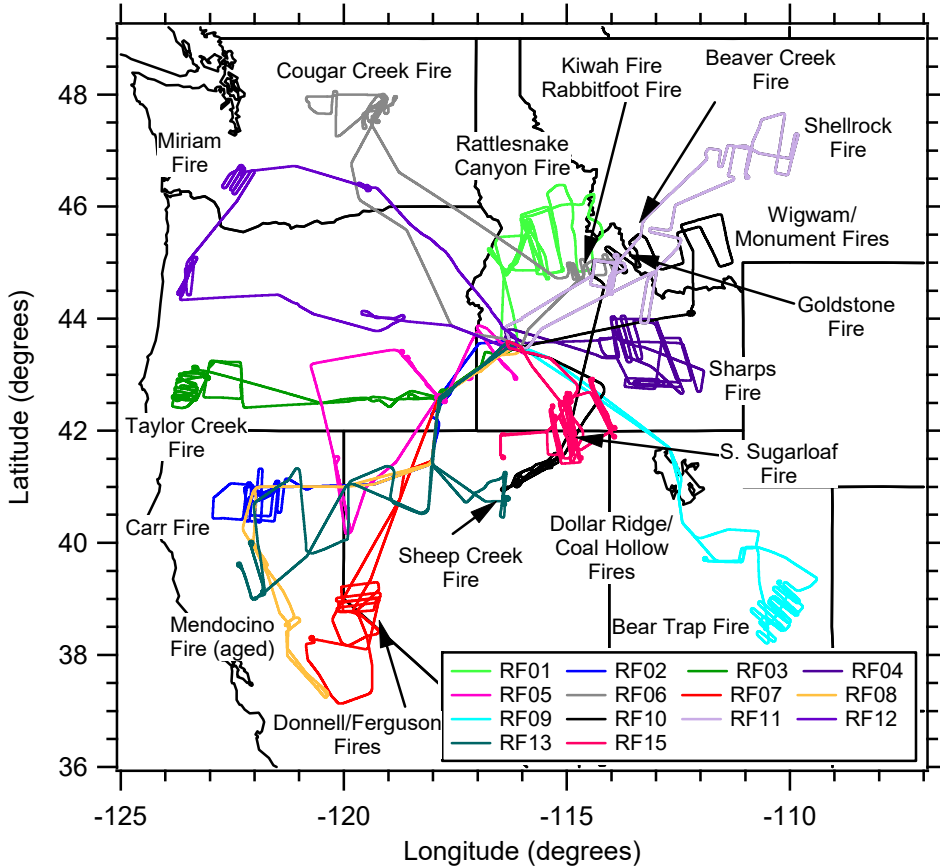
Figure 1. Map showing the flight paths and locations of the wildfires sampled during WE-CAN used in this analysis.

184
185
186
187 denuder [*Though et al.*, 1993] was situated upstream of both PILS to remove organic gases. In
188 addition, for PILS2 two honeycomb denuders coated with sodium carbonate and phosphorous
189 acid were used to remove inorganic acidic and basic gases in order to limit possible positive
190 artifacts from dissolving in the PILS collection liquid. PILS 1 was connected to a LWCC (liquid
191 waveguide capillary cell) and TOC (Total Organic Carbon) Analyzer for near real-time
192 measurement of water-soluble BrC (Brown Carbon) absorption and WSOC (water-soluble
193 organic carbon), respectively. PILS2 was coupled to a Bretchel fraction collector system
194 [*Sorooshian et al.*, 2006] to provide liquid samples for additional off-line analysis.
195   For PILS 1, a valve upstream of the PILS was manually closed periodically for 10 min
196 forcing the airflow through a Teflon filter allowing for a measurement of the background in near
197 real-time. The liquid sample obtained from PILS1 was then pushed through a 0.2 μm PTFE
198 liquid filter at a flowrate of 1.2 mL/min by a set of syringe pumps with 1 mL syringes to ensure
199 any insoluble particles were removed before passing through the LWCC and TOC Analyzer.
200   A LWCC with a 2.5 m path-length (World Precision Instruments, Sarasota, FL) was
201 employed. An absorption spectrometer (FLAME-T-UV-VIS, Ocean Optics, Largo, FL) and dual
202 deuterium and tungsten halogen light source (DH-mini, Ocean Optics, Largo, FL) were coupled
203 to the LWCC via fiber optic cables. The Oceanview Spectroscopy Software was used to record

204 absorption spectra over a range from 200 to 800 nm. In this paper we present the absorption
205 determined at 365 and 405 nm. This wavelength dependent absorption was calculated following
206 the method outlined in *Hecobian et al.* [2010]. A 16 s integrated measurement of water-soluble
207 absorption with a limit of detection (LOD) of 0.1 Mm^{-1} was obtained.
208   A Sievers Model M9 Portable TOC Analyzer (Suez Waters Analytical Instruments,
209 Boulder, CO) was used for the WSOC measurement. This analyzer converts organic carbon in
210 the liquid sample to carbon dioxide using chemical oxidation with ammonium persulfate and
211 ultraviolet light. The carbon dioxide formed is then measured by conductivity. The amount of
212 OC present in the sample is proportional to the increase in conductivity observed. The analyzer
213 was run in turbo mode providing a 4 s integrated measurement of WSOC with a LOD of 0.1 μg
214 C/m^3.
215   For PILS2, a valve upstream of the PILS was manually closed periodically for 10 min
216 forcing the airflow through a hepa filter allowing for measurement of the background in near
217 real-time. The liquid sample obtained from PILS2 was pushed into the fraction collector vials at
218 a flowrate of 0.65 mL/min by a peristaltic pump for collection of ~1.2 mL of liquid sample per
219 vial. Each fraction collector carousel holds 72 1.5 mL polypropylene vials (Microsolv
220 Technology Corporation, Leland, NC). Vials were fitted with pre-slit caps and used as supplied.
221 The fraction collector program was set to allow continuous collection of 2 min integrated
222 samples and was manually started after take-off. Carousels were pre-loaded before flight and
223 then manually switched out as they were filled. The vials were unloaded from the carousels at
224 the end of each flight, recapped with solid caps (Microsolv Technology Corporation), packed in
225 coolers with ice packs, and shipped back to Colorado State University to be stored in a 2 °C cold
226 room until analysis began following completion of the study.
227
228 **2.3. Off-line Analysis**
229   Each fraction collector vial was brought to room temperature and then analyzed for
230 anhydrosugars as well as cations. For each analysis, 300 μL aliquots were transferred to
231 polypropylene vials. Only levoglucosan, water-soluble potassium, and ammonium are discussed
232 here and their analytical methods are explained below.
233   The levoglucosan analysis was performed on a Dionex DX-500 series ion chromatograph
234 with pulsed amperometric detection via an ED-50/ED-50A electrochemical cell. This cell
235 includes two electrodes: a "standard" gold working electrode and pH-Ag/AgCl (silver/silver
236 chloride) reference electrode. A sodium hydroxide gradient and a Dionex CarboPac PA-1
237 column (4 x 250 mm) were employed for the separation. The complete run time was 59 min
238 with an injection volume of 100 μL. More details on the method can be found in *Sullivan et al.*
239 [2011a,b, 2014, 2019]. Only levoglucosan could be detected in the WE-CAN samples (other less
240 abundant anhydrosugars were too low to detect in the PILS samples) and did not require
241 background correction. The LOD for levoglucosan based on a sample collection time of 2 min
242 and air flowrate of 15 LPM was determined to be less than approximately 0.10 ng/m^3.
243   A Dionex ICS-3000 ion chromatograph equipped with a conductivity detector was used
244 to measure water-soluble potassium and ammonium. An eluent generator provided a
245 concentration of 20 mM methanesulfonic acid at a flowrate of 0.5 mL/min to perform the
246 separation on a Dionex IonPac CS12A analytical column (3 x150 mm). The complete run time
247 was 17 min with an injection volume of 190 μL. A blank correction was necessary for both of
248 these species unlike levoglucosan. Therefore, their concentrations were corrected by using the

249 average of all background samples collected during a specific flight. For water-soluble
250 potassium and ammonium, the LOD was 1 ng/m^3.
251
252 **2.4. Photoacoustic Aerosol Absorption Spectrometer**
253   A custom-built PAS was used to measure total aerosol absorption at 405 and 660 nm
254 [*Foster et al.*, 2019] every 1 s during WE-CAN. The PAS measures aerosol light absorption at
255 near-ambient conditions by heating particles using a controlled light source and detecting the
256 resulting soundwave. It can be subject to interference by gaseous absorbers and is sensitive to
257 variations in relative humidity, temperature, and pressure [*Arnott et al.*, 1999; *Langridge et al.*,
258 2013]. The PAS sampled from a Solid Diffuser Inlet (SDI) mounted on the front right side of the
259 NSF/NCAR C-130. Aerosol passed through a cyclone impactor before entering the PAS to
260 remove particles with aerodynamic diameters > 1 μm. The flowrate for the PAS was 4 LPM.
261 Upstream of the PAS was a denuder to remove NO$_x$ (nitrogen oxides) from the sample air as
262 well as a Perma Pure dryer to dry the aerosol to below 30% relative humidity. A filter was
263 periodically switched in-line before the PAS to remove particles and allow for a near real-time
264 measurement of the baseline stability. Additionally, the PAS switched between sampling with
265 and without a thermal denuder system in-line. Only the data from sampling without the thermal
266 denuder is presented here. The PAS BrC absorption at 405 nm (PAS total Abs 405 BrC) was
267 calculated using equation 9 from *Pokhrel et al.* [2017]. This approach assumes the absorption
268 determined by the PAS at 660 nm was equivalent to BC absorption, the BC aerosol AAE was 1,
269 and the absorption enhancement from lensing was constant at all wavelengths. Previous work
270 using this approach in smoke from controlled laboratory burns found lensing could contribute a
271 maximum of 30% of total absorption, but typical contributes much less.
272
273 **2.5. Ultra-High-Sensitivity Aerosol Spectrometer**
274   One second particle number concentrations were measured using a rack-mounted
275 UHSAS (Ultra-High-Sensitivity Aerosol Spectrometer). The rack-mounted UHSAS switched
276 between sampling from the SDI inlet and a CVI (counter-flow virtual impactor) when sampling
277 out of and in-cloud, respectively. We only present data for sampling out of clouds. The rack-
278 mounted UHSAS was operated so that the flow could be manually lowered by the in-flight
279 operator when the NSF/NCAR C-130 flew through smoke plumes to allow the UHSAS to stay
280 within its optimum concentration measurement range. The UHSAS measures particles in the
281 0.06-1 μm range. The particle size bins for the UHSAS were calibrated using ammonium sulfate
282 rather than traditional PSL (polystyrene latex) spheres. Particle mass concentrations for PM$_1$
283 were calculated by summing all size bins and then multiplying by 1.4 g/cm^3 to account for
284 particle density.
285
286 **2.6. Other Measurements**
287   In the following analysis, we focus on characterizing the BrC absorption in smoke from
288 wildfires in the western U.S. sampled during WE-CAN. Other airborne measurements used in
289 this analysis include meteorological data and coordinates provided by the Research Aviation
290 Facility (RAF) as part of the C-130 instrumentation package
291 (https://data.eol.ucar.edu/project/WE-CAN) and one Hz carbon monoxide (CO) determined by a
292 vacuum UV (ultraviolet) resonance fluorescence method [*Gerbig et al.*, 1999]. All data
293 presented in our analysis are reported at 1 atm and 273 K. Data from all species have been
294 averaged to match the 2 min collection time of the PILS-fraction collector system.

295
296 **2.7. Mie Calculation**
297   Mie calculations were performed by putting the complex refractive index (m = n+ ik) into
298 Mie code to obtain the absorption efficiency (Q) and then further calculate the absorption
299 coefficient using Eq. 1 [*Liu et al.*, 2013]. The real part of the refractive index (n) was set to be
300 1.55 and the imaginary part was calculated using Eq. 2 [*Liu et al.*, 2013].
301

302 $$\beta\left(\lambda, D_p\right) = \frac{3}{2} \cdot \frac{Q \cdot WSOC}{D_p \cdot \rho} \qquad (Eq.\,1)$$

303

304 $$k = \frac{\rho\lambda \cdot H_2O\_\beta(\lambda)}{4\pi \cdot WSOC} \qquad (Eq.\,2)$$

305

306 In Eq. 1 and 2, λ is the wavelength, D_p is the diameter of the particle, β is the absorption
307 coefficient (referred to as the Mie calculated water-soluble absorption hereinafter), Q is the
308 absorption efficiency, $WSOC$ is the water-soluble organic carbon mass concentration measured
309 by the PILS, and $H_2O\_\beta(\lambda)$ is the water-soluble light absorption coefficient measured by the
310 PILS. The particle density (ρ) was assumed to be 1.4 g/cm^3. The plume averaged particle size
311 distribution (measured by the UHSAS) was used in the calculation. The Mie calculated water-
312 soluble absorption was determined for each size bin in order to obtain the most accurate results.
313 Mie calculated total absorption was further calculated by multiplying the Mie calculated water-
314 soluble absorption by (UHSAS mass)/(WSOC*1.6), where the factor of 1.6 was to convert
315 WSOC to WSOM (water-soluble organic matter) [*Duarte et al.*, 2019; *Yttri et al.*, 2007].
316
317 **3. Results and Discussion**
318 **3.1. Overview**
319   Most previous studies employing a LWCC to determine water-soluble absorption,
320 examine the absorption at 365 nm (e.g., [*Hecobian et al.*, 2010; *Zhang et al.*, 2011, 2013]). But
321 here in order to explore the relationship between the water-soluble and total absorption
322 determined by the PILS and PAS, respectively, we focus on the absorption at 405 nm determined
323 by the LWCC. Using as examples Flight RF02, which sampled the Carr Fire smoke plume, and
324 Flight RF11, which sampled the Goldstone, Rabbit Foot, Beaver Creek, and Shellrock Fire
325 smoke plumes, Figures 2a and b show the relationship of the PILS water-soluble Abs 405 vs.
326 Abs 365. Absorption values at these two wavelengths are correlated (R^2 values from 0.70 to
327 1.00 based on all individual WE-CAN Flights), but the absorption measured at 405 nm was
328 about half of that observed at 365 nm (slope average 0.45 and range from 0.39 to 0.52 across all
329 individual WE-CAN flights). We selected these two flights to cover the range in the
330 relationships observed during WE-CAN. The lower correlation for Flight RF11 is likely due to
331 the narrower plumes being sampled compared to the broader plumes observed in Flight RF02.
332 This difference related to narrow vs. broad plumes was observed throughout the various wildfires
333 sampled during WE-CAN.
334   Figure 3 shows example time series for WSOC, PILS water-soluble Abs 405, and PAS
335 total Abs 405 BrC from the same two flights as above. It was observed that all three parameters
336 tracked each other in and out of the smoke plumes. During WE-CAN, the average value ±
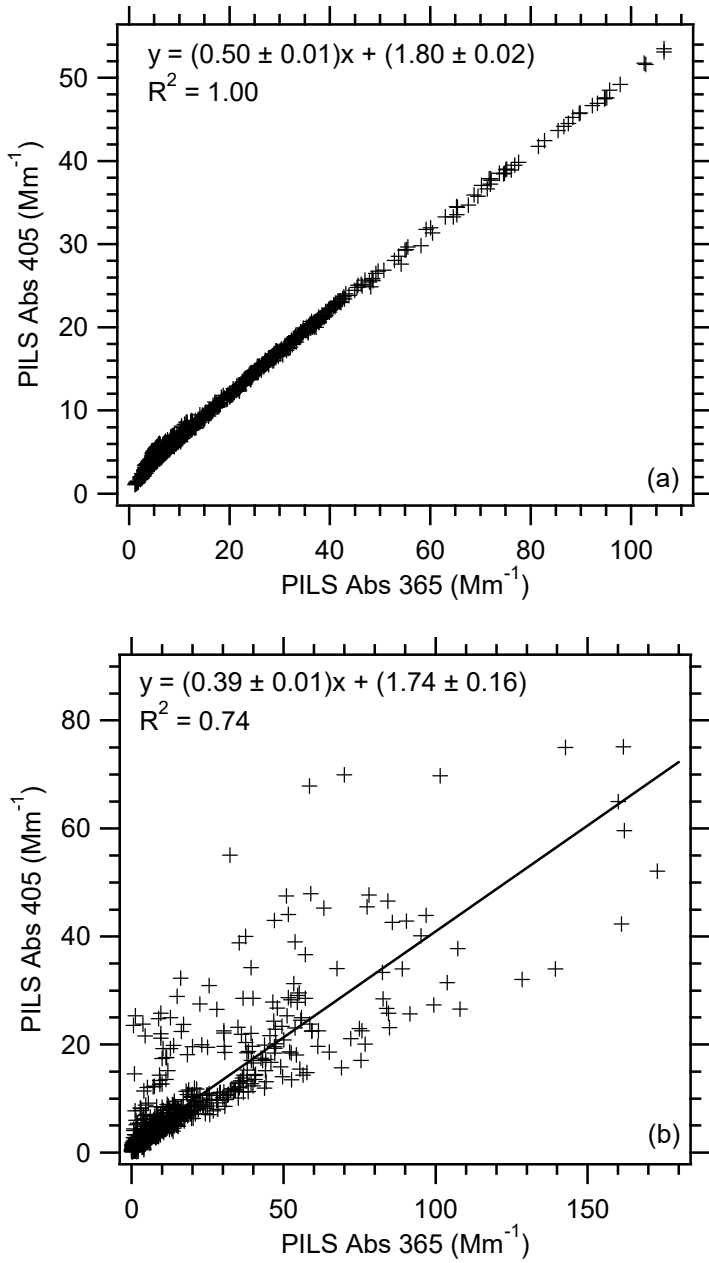
Figure 2. Correlation of PILS water-soluble Abs 405 vs. PILS water-soluble Abs 365 for WE-CAN (a) Flight RF02 and (b) Flight RF11. Uncertainties with the least square regressions are one standard deviation.

337
338
339
340
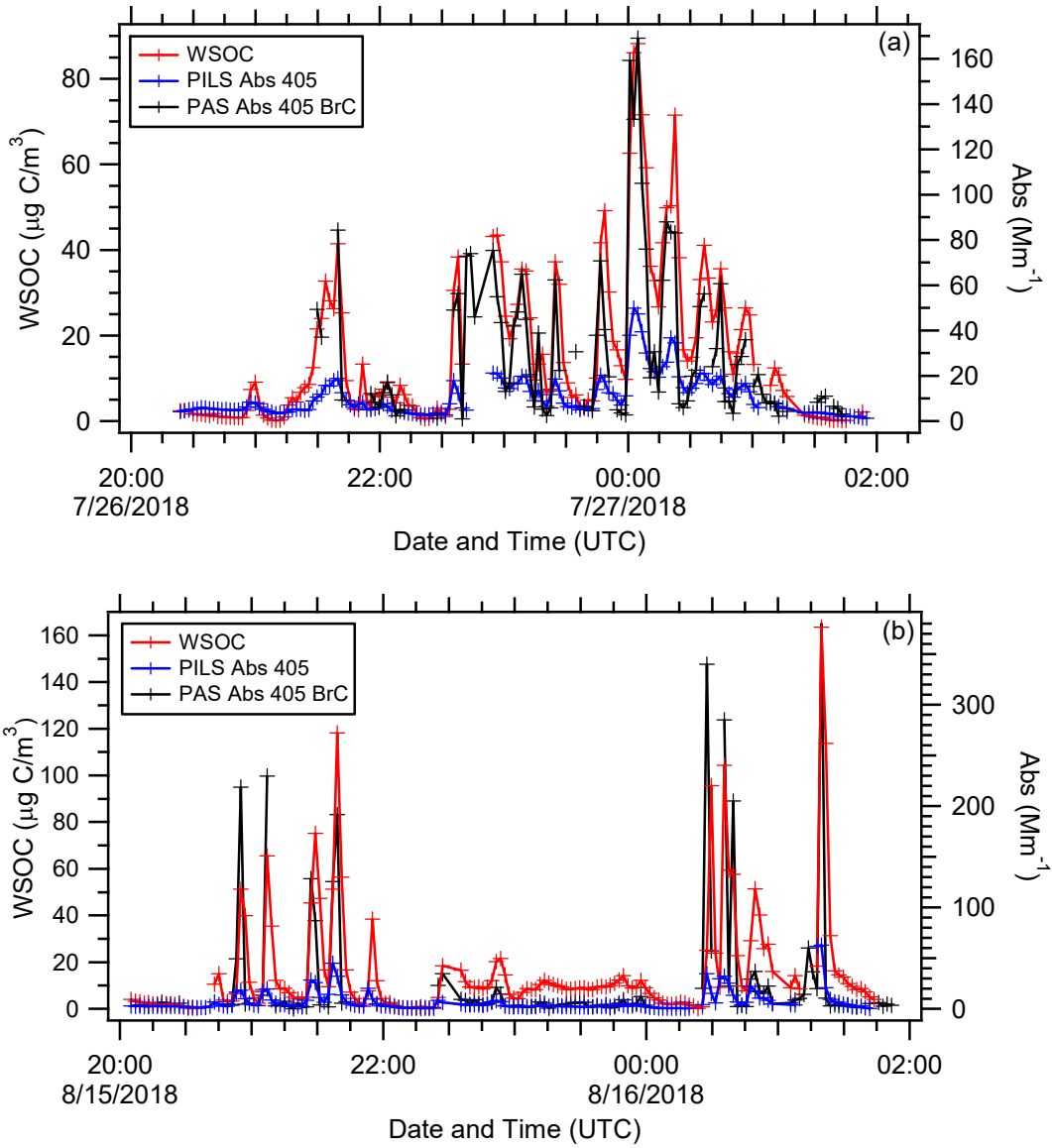
Figure 3. Time series of WSOC, PILS water-soluble Abs 405, and PAS total Abs 405 BrC for WE-CAN (a) Flight RF02 and (b) Flight RF11.

341

342

343

344 standard deviation for WSOC, PILS water-soluble Abs 405, and PAS total Abs 405 BrC were
345 13.35 ± 16.80 µg C/m^3, 6.06 ± 6.88 Mm^{-1}, and 22.02 ± 49.16 Mm^{-1}, respectively. The water-
346 soluble absorption determined by the PILS was lower than the total absorption determined by the
347 PAS. This pattern was consistently observed for all the wildfires sampled throughout WE-CAN.

348

349 **3.2. Relationship between Total and Water-Soluble BrC Absorption**
350   To further explore the relationship between total and water-soluble BrC absorption, we
351 examine the relationship between PAS total Abs 405 BrC and UHSAS mass for Flights RF02
352 and RF11. There is a strong correlation between PAS total Abs 405 BrC and UHSAS mass

353 (Figure 4). Therefore, the PILS water-soluble Abs 405 can be corrected for the non-water-
354 soluble fraction of the aerosol using the UHSAS mass. This was achieved by multiplying the
355 PILS water-soluble Abs 405 by 1/((WSOC*1.6)/(UHSAS mass)) or (UHSAS
356 mass)/(WSOC*1.6). This approach assumes the characteristics of the non-water-soluble
357 components of OC are identical to that of the water-soluble components of OC.
358   Correcting the PILS water-soluble Abs 405 by the UHSAS mass showed good closure
359 with the PAS total Abs 405 BrC, but with a factor of ~1.5 to 2 difference between the PILS
360 water-soluble Abs 405 corrected and PAS total Abs 405 BrC (Figures 4c and d). This is also
361 similar to results obtained from the sampling of wildfire smoke during the FIREX (Fire Influence
362 on Regional and Global Environments Experiment) Campaign, where there was a ratio of 3.2
363 between PAS Abs 405 BrC and water-soluble Abs 405 determined from off-line LWCC analysis
364 of filter samples [*Zeng et al.*, 2020]. This factor difference in both the WE-CAN and FIREX
365 data is likely due to the differences in particle vs. bulk solution absorption measured by the PAS
366 vs. LWCC (using PILS or filter samples), respectively, and can be explained by Mie Theory.
367   We used Mie Theory to calculate the water-soluble and total particle Abs 405 (see section
368 2.7 for details on the equations and parameters used) through each plume transect for RF02 and
369 RF11. As shown in Figures 5a and b, we found a slope of 1.7 to 1.8 for Mie calculated water-
370 soluble Abs 405 to PILS Abs 405 and 3 to 4 for Mie calculated total Abs 405 to PILS Abs 405.
371 This is similar to results presented in *Liu et al.* [2013] and based on off-line LWCC analysis of
372 filter samples collected at 3 sites in Georgia. In that work, a ratio of 2 for Mie calculated water-
373 soluble Abs 365 to measured water-soluble Abs 365 and a ratio of 3.6 for Mie calculated total
374 Abs 365 to measured water-soluble Abs 365 were observed. In *Zeng et al.* [2022], Mie Theory
375 was used to calculate the factor to convert solution to particle light absorption (i.e., ratio of Mie
376 calculated to measured water-soluble absorption) as a function of wavelength for the FIREX
377 data. At 405 nm a factor of ~1.7 was determined, similar to what was determined from the WE-
378 CAN data.
379   As a further check on the calculations performed here, the PAS Abs 405 BrC was
380 compared to the Mie calculated total Abs 405. Slopes ranged from 1.04 to 1.08 (Figures 5c and
381 d). This suggested our approach for correcting the PILS water-soluble Abs 405 for the non-
382 water-soluble fraction as well as to calculate the BrC absorption from the PAS Abs 405 data
383 were valid.
384   Overall, during WE-CAN ~45% (ranging from 31% to 65%) of the BrC absorption at
385 Abs 405 was due to water-soluble species. This is similar to what was observed from off-line
386 LWCC analysis of water and methanol extracts from filter samples collected during sampling of
387 biomass burning plumes as part of the DC3 (Deep Convective Clouds and Chemistry),
388 SEAC4RS (Studies of Emissions, Atmospheric Composition, Clouds and Climate Coupling by
389 Regional Surveys), and FIREX aircraft campaigns [*Forrister et al.*, 2015; *Liu et al.*, 2015; *Zeng
390 et al.*, 2022].
391
392 **3.3. BrC Absorption, CO, WSOC, and Levoglucosan**
393   Using data from all WE-CAN flights, Figure 6 shows that the PAS total Abs 405 BrC and
394 PILS water-soluble Abs 405 are correlated with CO (R^2 value for PAS = 0.76 and PILS = 0.55).
395 This further illustrates the importance of biomass burning as a source of BrC absorption (e.g.,
396 [*Andreae and Gelencsér*, 2006; *Chakrabarty et al.*, 2010; *Duarte et al.*, 2005; *Hecobian et al.*,
397 2010; *Hoffer et al.*, 2006; *Lack et al.*, 2012; *Lukács et al.*, 2007]), especially since more than
398 75% of the WE-CAN data occurred in smoke.
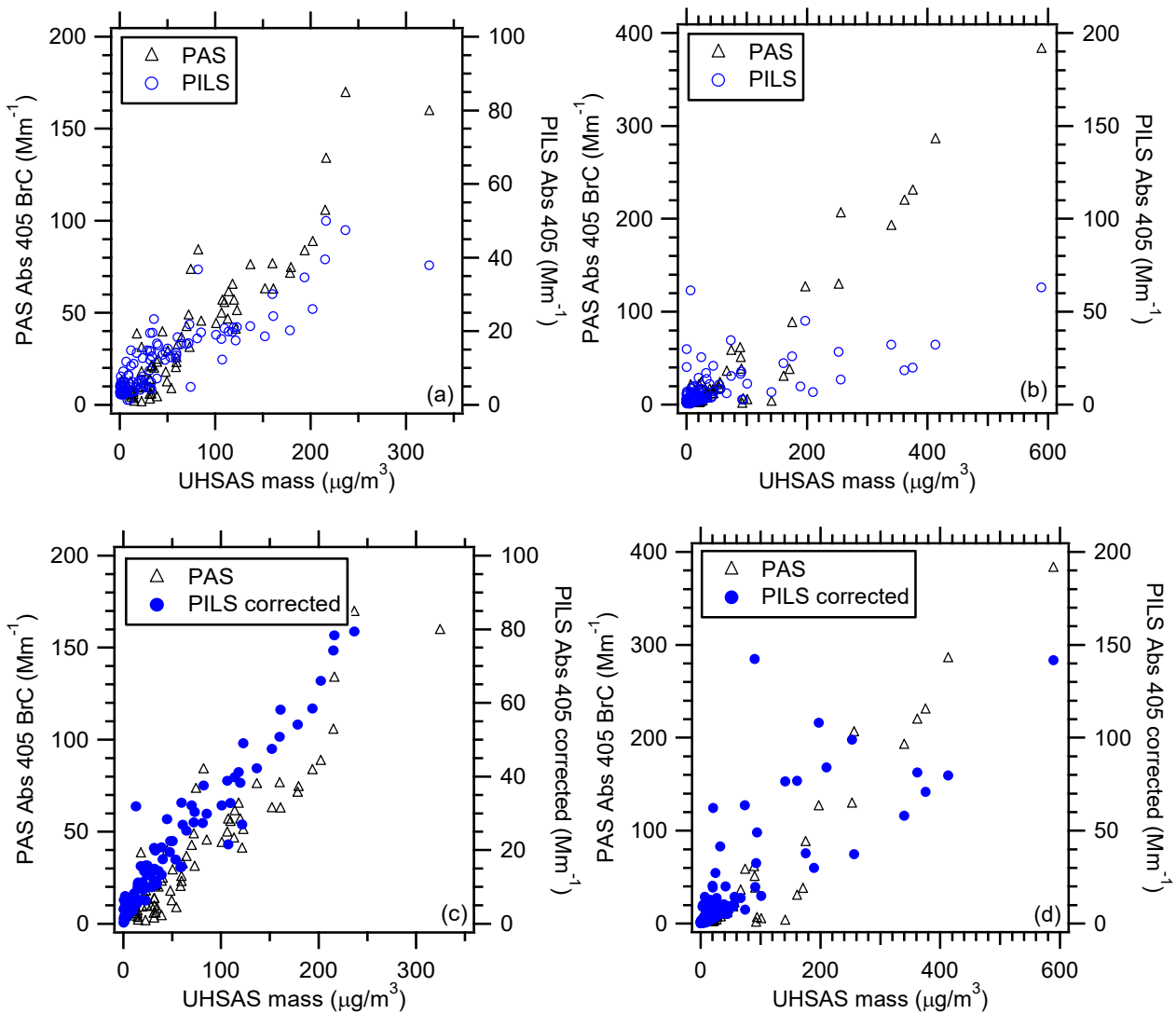
Figure 4. Correlation of PAS total Abs 405 BrC and PILS water-soluble Abs 405 vs. UHSAS mass for WE-CAN (a) Flight RF02 and (b) Flight RF11. Correlation of PAS total Abs 405 BrC and PILS water-soluble Abs 405 corrected for the non-water-soluble fraction of the aerosol using the UHSAS mass for WE-CAN (c) Flight RF02 and (d) Flight RF11. In plot (a), the equations for the fit and R^2 value for PAS are $y = (0.50 \pm 0.02)x - (0.03 \pm 2.29)$, $R^2 = 0.87$ and for PILS are $y = (0.14 \pm 0.01)x + (5.58 \pm 0.65)$, $R^2 = 0.75$, respectively. In plot (b), the equations for the fit and R^2 value for PAS are $y = (0.62 \pm 0.03)x - (6.09 \pm 3.62)$, $R^2 = 0.76$ and for PILS are $y = (0.08 \pm 0.01)x + (3.58 \pm 0.66)$, $R^2 = 0.43$, respectively. In plot (c), the equation for the fit and R^2 value for PILS are $y = (0.32 \pm 0.01)x + (3.60 \pm 0.68)$, $R^2 = 0.94$, respectively. In plot (d), the equation for the fit and R^2 value for PILS are $y = (0.24 \pm 0.01)x + (2.93 \pm 1.35)$, $R^2 = 0.65$, respectively. Uncertainties with the least square regressions are one standard deviation.

399
400
401
402
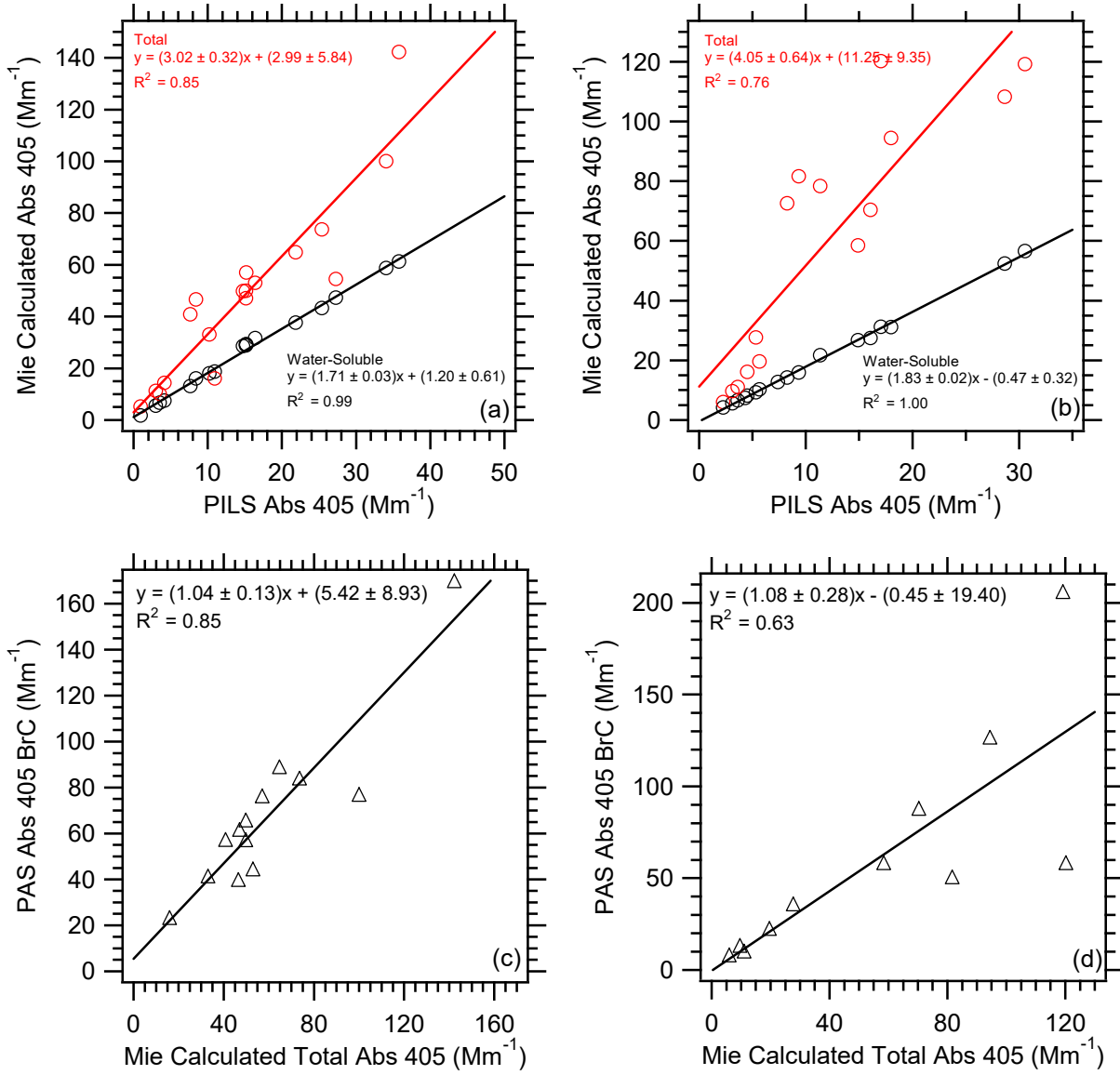
Figure 5. Correlation of Mie calculated water-soluble and total Abs 405 vs. PILS water-soluble Abs 405 for WE-CAN (a) Flight RF02 and (b) Flight RF11. Correlation of PAS total Abs 405 BrC and Mie calculated total Abs 405 for WE-CAN (c) Flight RF02 and (d) Flight RF11. Uncertainties with the least square regressions are one standard deviation.

403

404

405

406   Figure 7 shows that there is a correlation between BrC absorption and WSOC (R^2 value
407   for PAS = 0.42 and PILS = 0.60). This is not surprising given that the two main sources of
408   WSOC are typically biomass burning and secondary organic aerosol (SOA) [*Sullivan et al.*,
409   2006]. A number of previous studies where the source of WSOC and Abs 365 was one or both
410   of these have observed a similar correlation (e.g., [*Hecobian et al.*, 2010; *Liu et al.*, 2015; *Zhang
411   et al.*, 2013]).

412
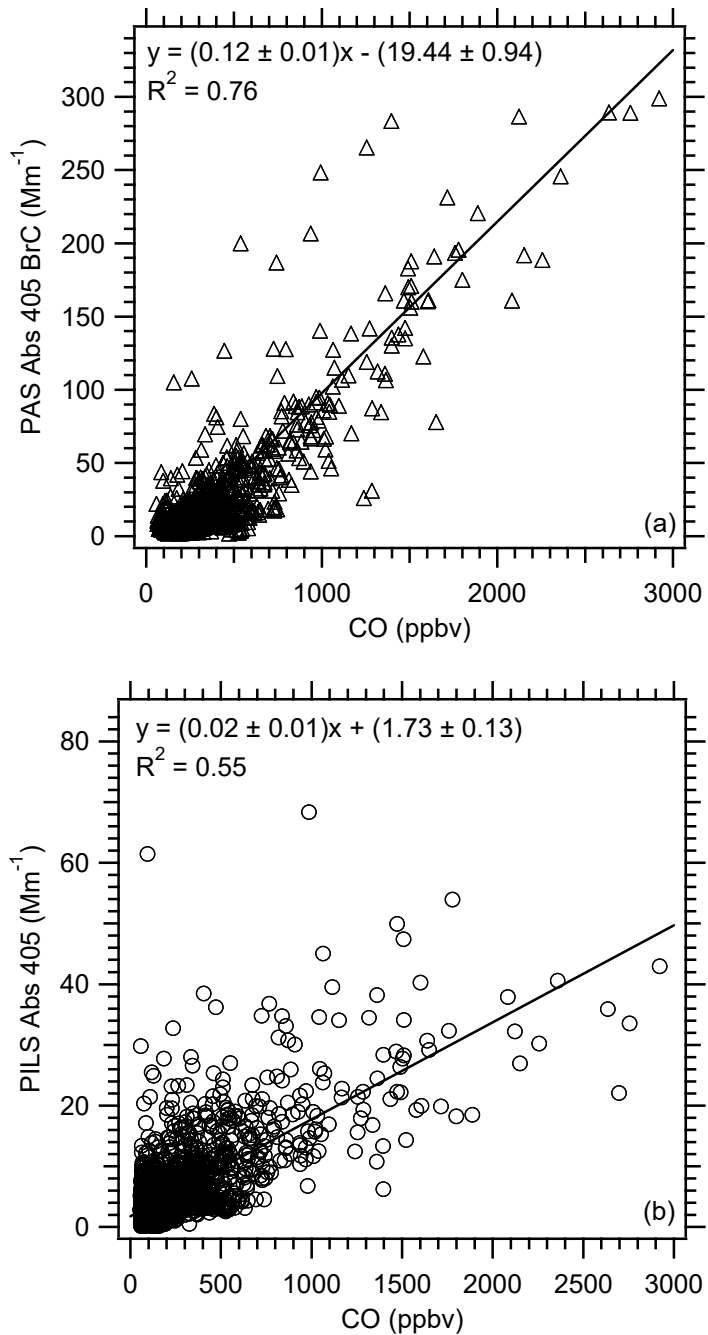
Figure 6. Correlation of (a) PAS total Abs 405 BrC and (b) PILS water-soluble Abs 405 vs. CO for all WE-CAN flights used in this analysis. Uncertainties with the least square regressions are one standard deviation.

413

414

415

416   BrC absorption has a similar relationship with CO and WSOC as the biomass burning

417   marker levoglucosan [*Simoneit et al.*, 1999], but there are additional features (Figure 8). There is

418   some variability in the ratio of levoglucosan to the PAS total Abs 405 BrC and PILS water-
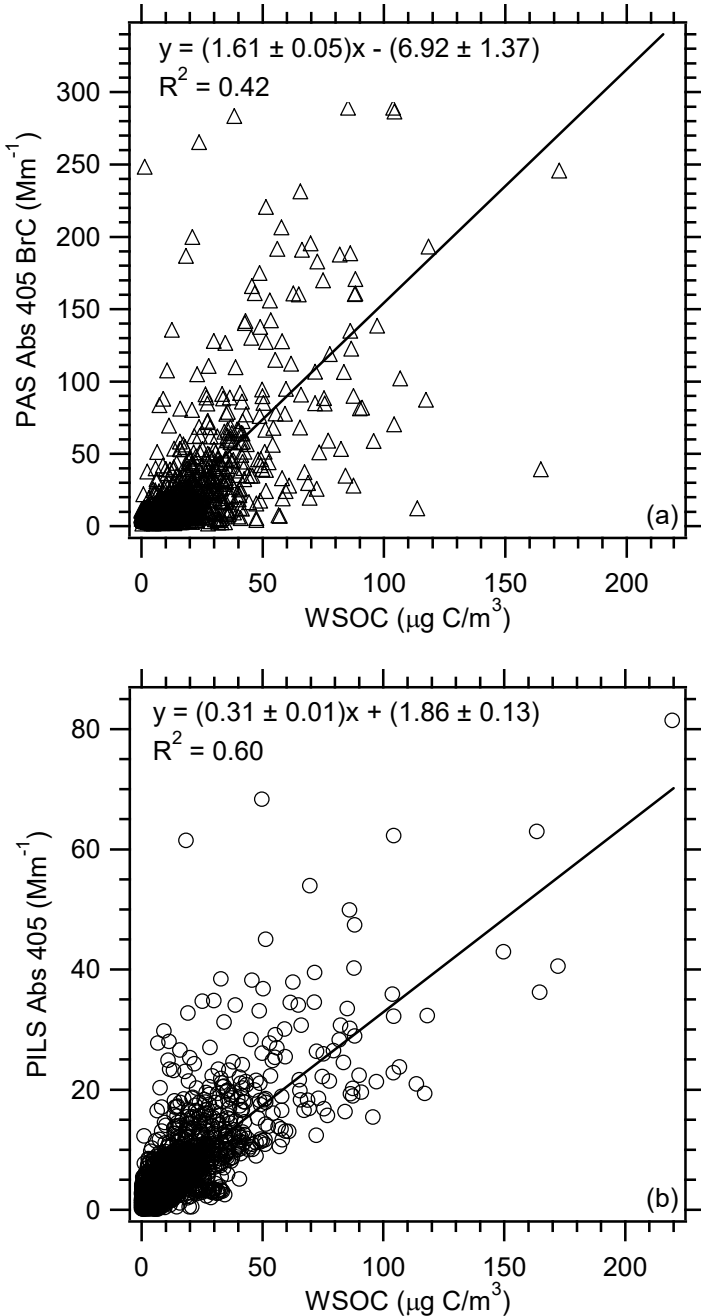
Figure 7. Correlation of (a) PAS total Abs 405 BrC and (b) PILS water-soluble Abs 405 vs. WSOC for all WE-CAN flights used in this analysis. Uncertainties with the least square regressions are one standard deviation.

419
420
421
422   soluble Abs 405 between wildfires, and this leads to two branches (Branch 1 and Branch 2).
423   This was also observed for levoglucosan vs. WSOC (not shown). While there is no overall
424   correlation of levoglucosan vs. BrC absorption across all flights, there are correlations between
425   these two species on an individual flight basis (e.g., R^2 value for Flight RF02 = 0.76 and Flight
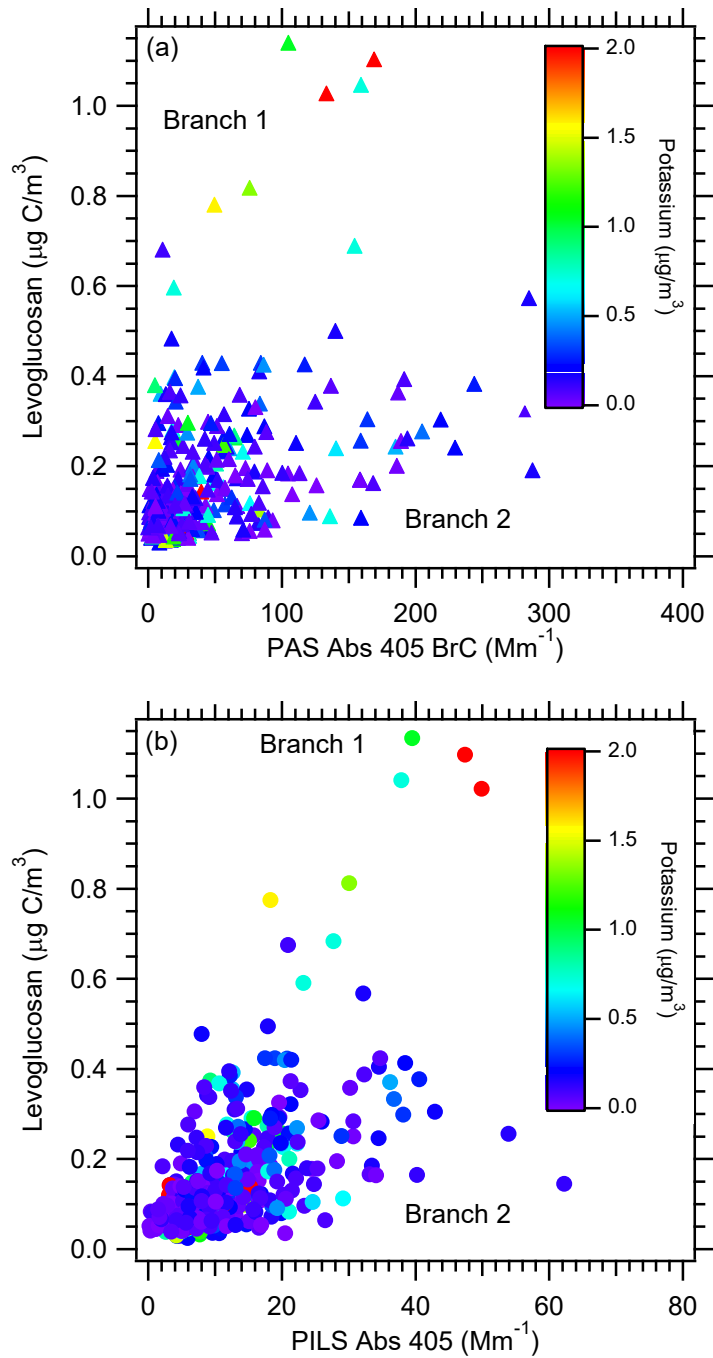
Figure 8. Correlations of levoglucosan on a carbon mass basis vs. (a) PAS total Abs 405 BrC and (b) PILS water-soluble Abs 405 for all WE-CAN flights used in this analysis with the data colored by the PILS water-soluble potassium concentrations. Branch 1 represents data with water-soluble potassium concentrations > 0.5 $\mu g/m^3$ and Branch 2 < 0.5 $\mu g/m^3$. In plot (a), the equation for the fit and R^2 value for Branch 1 are $y = (0.006 \pm 0.001)x + (0.027 \pm 0.049)$, $R^2 = 0.60$ and for Branch 2 $y = (0.001 \pm 0.001)x + (0.118 \pm 0.006)$, $R^2 = 0.22$, respectively. In plot (b), the equation for the fit and R^2 value for Branch 1 are $y = (0.024 \pm 0.002)x - (0.081 \pm 0.038)$, $R^2 = 0.76$ and for Branch 2 $y = (0.006 \pm 0.001)x + (0.073 \pm 0.007)$, $R^2 = 0.35$, respectively. Uncertainties with the least square regressions are one standard deviation.

426   RF11 = 0.60, not shown). When data from all flights are colored by the water-soluble potassium
427   concentration, we observe that Branch 1, which had the highest levoglucosan concentrations,
428   also has the highest water-soluble potassium concentrations (> 0.5 μg/m^3). Levoglucosan and
429   BrC absorption are much more highly correlated in Branch 1, than in Branch 2 for both the PILS
430   (R^2 values Branch 1 = 0.76 and Branch 2 = 0.35) and PAS (R^2 values Branch 1 = 0.60 and
431   Branch 2 = 0.22) BrC absorption. To further examine this, the times series of PILS water-
432   soluble Abs 405, levoglucosan, potassium, and ammonium for Flights RF02 and RF11 are shown
433   in Figure 9. Smoke impacted samples in Flight RF02 had higher concentrations of levoglucosan
434   and water-soluble potassium and contributed to Branch 1. The data from Flight RF11
435   contributed to Branch 2. In addition, elevated water-soluble potassium was observed in many of
436   the plume intercepts during Flight RF02. But more elevated ammonium was observed for Flight
437   RF11, which became even more prominent in smoke intercepts after 00:00 UTC, while water-
438   soluble potassium was relatively less abundant. While ammonium was clearly more prominent,
439   there was no correlation observed between ammonium and PAS total Abs 405 BrC or PILS
440   water-soluble Abs 405 for the data contributing to Branch 2 (not shown). Water-soluble
441   potassium is a known inorganic marker for biomass burning, although it is not as specific of a
442   marker as levoglucosan as there are additional possible sources for water-soluble potassium
443   [*Schauer et al.*, 2001] and water-soluble potassium is predominately emitted during only the
444   flaming phase of a fire [*Lee et al.*, 2010]. It is possible this difference in timing of emissions is
445   what leads to the different relationship of Abs 405 with levoglucosan than was observed for CO
446   and WSOC. It has been observed in previous work looking at the size-resolved aerosol
447   composition and single particle measurements from wildfire plumes that water-soluble potassium
448   and levoglucosan appear in different sized particles than BrC and that there is non-uniform
449   mixing of them [*Di Lorenzo et al.*, 2018; *Lee et al.*, 2016], which could also be a factor. These
450   results from WE-CAN are further suggesting there may be a relationship between levoglucosan
451   and water-soluble potassium in wildfire emissions that has not been observed in other types of
452   burning, such as prescribed burning, residential burning, or controlled laboratory burns [*Sullivan*
453   *et al.*, 2014, 2019].
454
455   **3.4. Evolution of BrC Absorption with Plume Age and Fire Dynamics**
456   The time since emission (i.e., the smoke age) was estimated for all possible wildfire
457   plumes as the distance the plume was sampled from the source divided by the average wind
458   speed at that particular sampling altitude. Only PILS-fraction collector samples that directly
459   overlapped with a CO plume penetration are considered. To account for dilution, we normalized
460   the BrC absorption to 3 different species. We examine the ratio of BrC absorption to WSOC,
461   ΔCO (assuming a CO background of 100 ppbv), and levoglucosan.
462   Figure 10a presents the ratio of PAS total Abs 405 BrC to WSOC and PILS water-soluble
463   Abs 405 to WSOC, Figure 10b presents the ratio of PAS total Abs 405 BrC to ΔCO and PILS
464   water-soluble Abs 405 to ΔCO, and Figure 10c presents the ratio of PAS total Abs 405 BrC to
465   levoglucosan and PILS water-soluble Abs 405 to levoglucosan as a function of time since
466   emission. To better discern any trends, Figures S1-S3 show these 3 ratios for each smoke plume
467   on an individual flight basis. If WSOC was lost with age due to evaporation of more volatile
468   components or SOA formation were occurring with time since emission, CO would be expected
469   to be more stable. It appears, however, that a similar pattern, perhaps with a bit more scatter for
470   Abs 405 to WSOC, is observed for all of these ratios. Within a particular wildfire, there is no
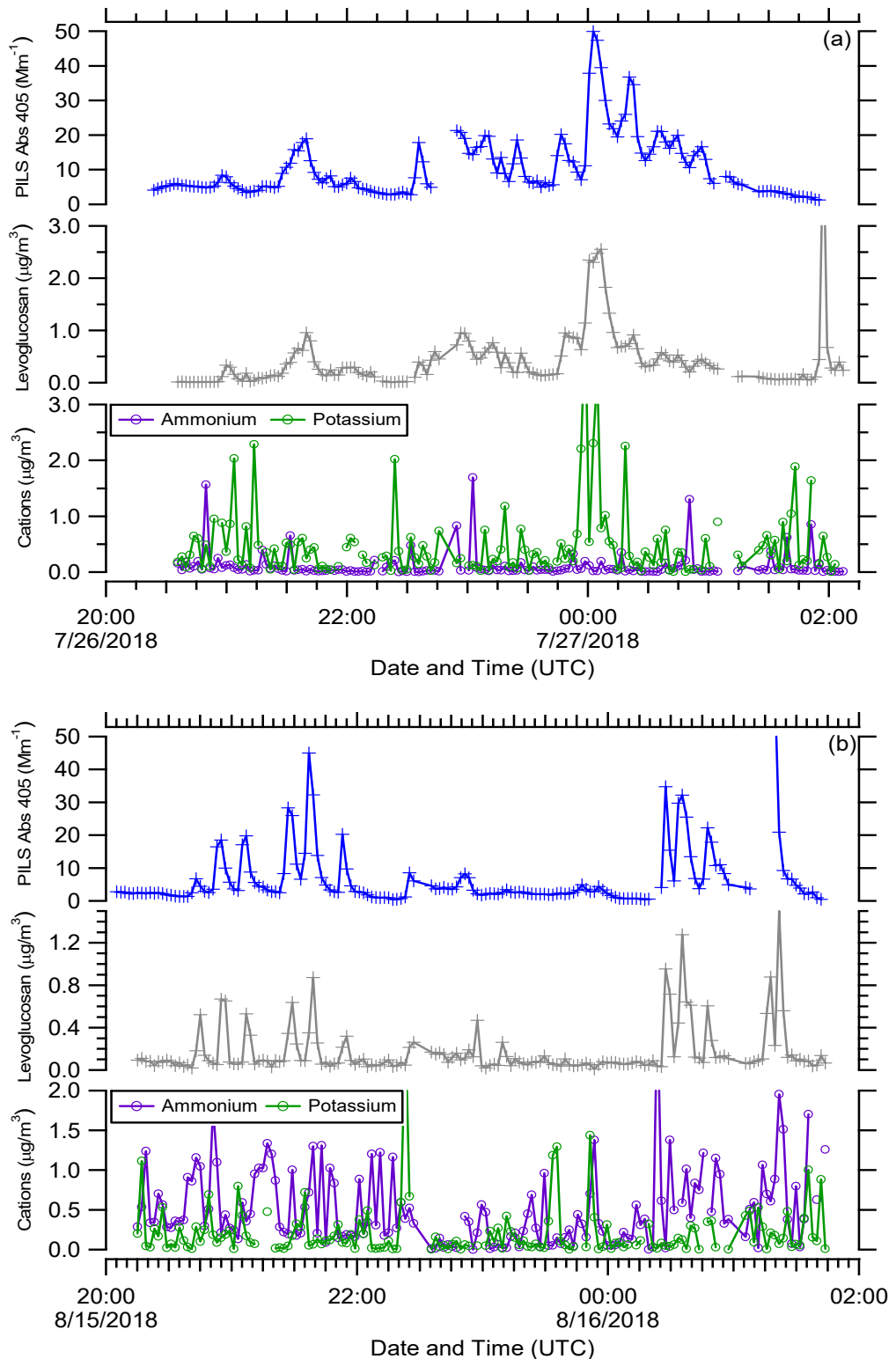
Figure 9. Time series from top to bottom of PILS water-soluble Abs 405, PILS levoglucosan, and PILS ammonium and water-soluble potassium for WE-CAN (a) Flight RF02 and (b) Flight RF11.

471
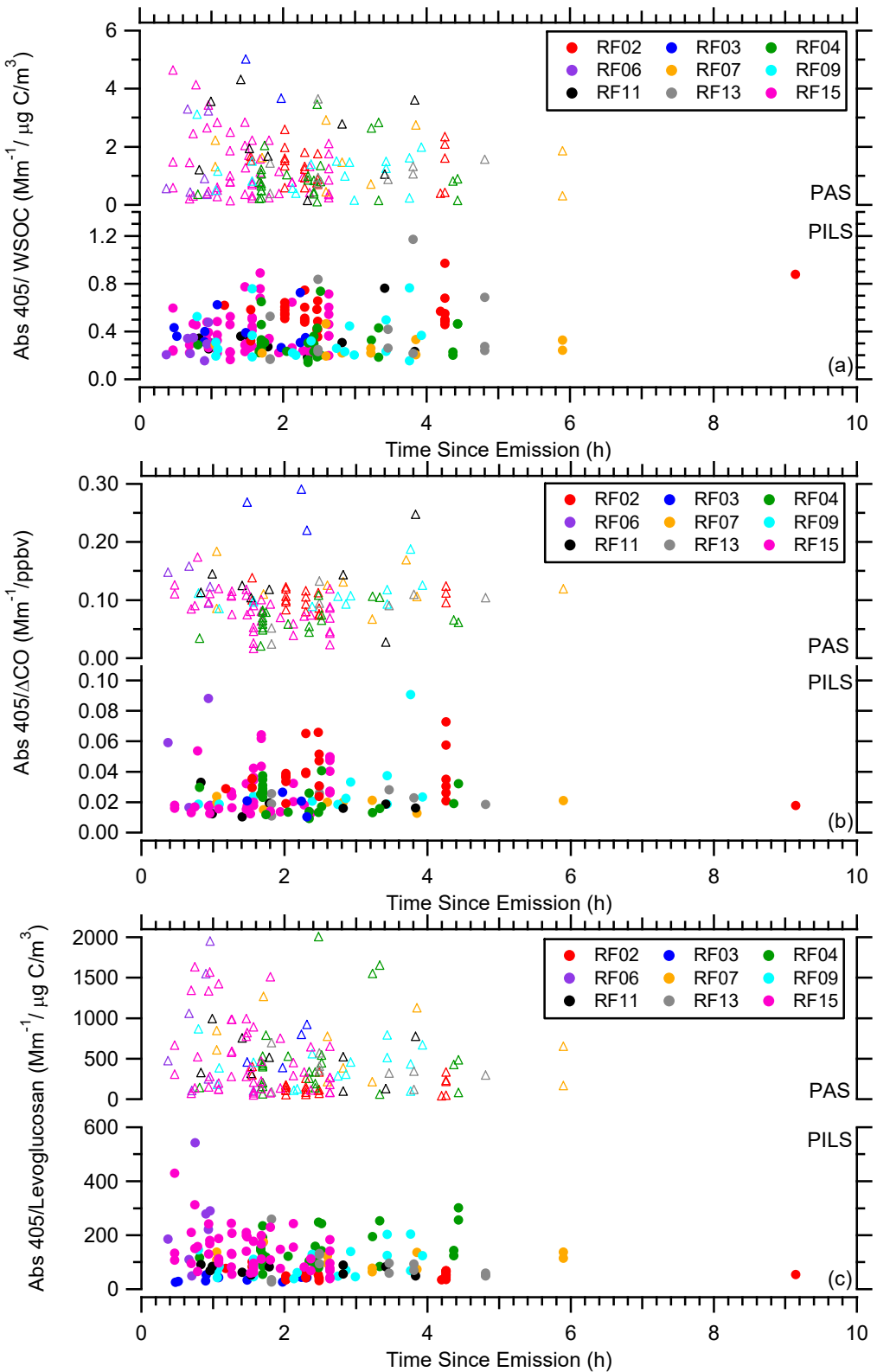
Figure 10. (a) Abs 405/WSOC, (b) Abs 405/ΔCO, and (c) Abs 405/levoglucosan as a function of time since emission for all WE-CAN flights with the data segregated by flight. In each plot the PAS total Abs 405 BrC is on top and the PILS water-soluble Abs 405 on the bottom.

472   clear evidence that the PILS water-soluble BrC absorption is affected by smoke age up to 9 h.
473   For the PAS total BrC absorption, especially for the ratio to ΔCO, there appears to be a possible
474   decrease in the ratio in the first 2 h (see Figures S1i and S2i for Flight RF15 which best covered
475   this period), suggesting a need to further explore changes in total BrC absorption near the source
476   region.
477   A number of laboratory studies suggest the initial stages of photochemical aging
478   increases light absorption (i.e., photoenhancement). This is then followed by a decrease in light
479   absorption (i.e., photobleaching) [*Hems and Abbatt*, 2018; *Saleh et al.*, 2013; *Sumlin et al.*, 2017;
480   *Zhao et al.*, 2015; *Zhong and Jang*, 2014]. However, it is challenging to directly compare this
481   laboratory data to the ambient data collected during WE-CAN. But analysis of laboratory and
482   ambient biomass burning samples found low molecular weight (< 400 Da) BrC undergoes rapid
483   photobleaching on timescales of a few h, but high molecular weight (> 400 Da) BrC was stable
484   for up to a few days [*Di Lorenzo et al.*, 2017; *Wong et al.*, 2019]. This suggests that the BrC
485   sampled during WE-CAN could be composed mainly of high molecular weight species.
486   In addition, to investigate these ratios as a function of time since emission, the WE-CAN
487   data had to be integrated across a smoke plume in order to incorporate the PILS-fraction
488   collector measurements. Of course, a smoke plume itself was dynamic with concentrations
489   being highest in the middle of the plume and more dilute on the edges. It is possible the
490   averaging could contribute to the observed pattern of BrC absorption not changing with age.
491   *Forrister et al.* [2015], who used plume transect averages of SEAC4RS data, reported a decrease
492   in the total Abs 365/ΔCO from ~0.13 to 0.07 Mm^{-1}/ppbv in 5 h for smoke from the Rim Fire.
493   Observations of smoke during FIREX, by contrast, indicated no clear trend with plume age
494   [*Washenfelder et al.*, 2022; *Zeng et al.*, 2022] in a dataset where the majority of plume ages were
495   less than 10 h. These varying results also suggest that other factors that contribute to changes in
496   BrC absorption over time may still need to be explored.
497   As these three studies all examined Abs 365, the same series of plots shown in Figure 10
498   are repeated for PILS water-soluble Abs 365 and shown in Figure S4. A similar pattern was
499   observed at both wavelengths for the WE-CAN data. This suggests our results were not
500   wavelength specific and further corroborate the results observed during FIREX.
501   An analysis of WE-CAN data by *Palm et al.* [2020] looking at the evolution of organic
502   aerosol and BrC suggested that although changes in organic aerosol were likely occurring, there
503   was a balance between dilution-driven evaporation and subsequent formation resulting in little
504   change over time. It is hard to compare these results to our analysis as the *Palm et al.* [2020]
505   work chose to focus only on the total organic aerosol and total Abs 405 BrC and did not examine
506   the WSOC or water-soluble Abs 405. When examining the ratio of WSOC to ΔCO as a function
507   of time since emission (Figure S5) during WE-CAN, there was not clear evidence for formation
508   or loss of WSOC being observed within a particular wildfire. But a recent analysis by *Zeng et al.*
509   [2022] has shown in wildfire plumes that dilution-drive evaporation was likely playing a minor
510   role compared to the effects of ozone on BrC.
511   In order to investigate the possible influence of fire dynamics on BrC absorption, the
512   modified combustion efficiency (MCE) was calculated as the change in carbon dioxide divided
513   by the sum of the change in carbon monoxide and carbon dioxide ($\Delta CO_2/(\Delta CO +\Delta CO_2)$) on a
514   molar basis [*Ward and Radke*, 1993]. A higher MCE value indicates a more intense or extended
515   flaming phase as opposed to a smoldering phase. Within a particular wildfire there appeared to
516   be no clear dependence of the ratio of BrC absorption to WSOC, ΔCO, or levoglucosan on MCE
517   (Figure 11 and Figures S6-S8), except that an overall lower Abs 405/levoglucosan ratio was
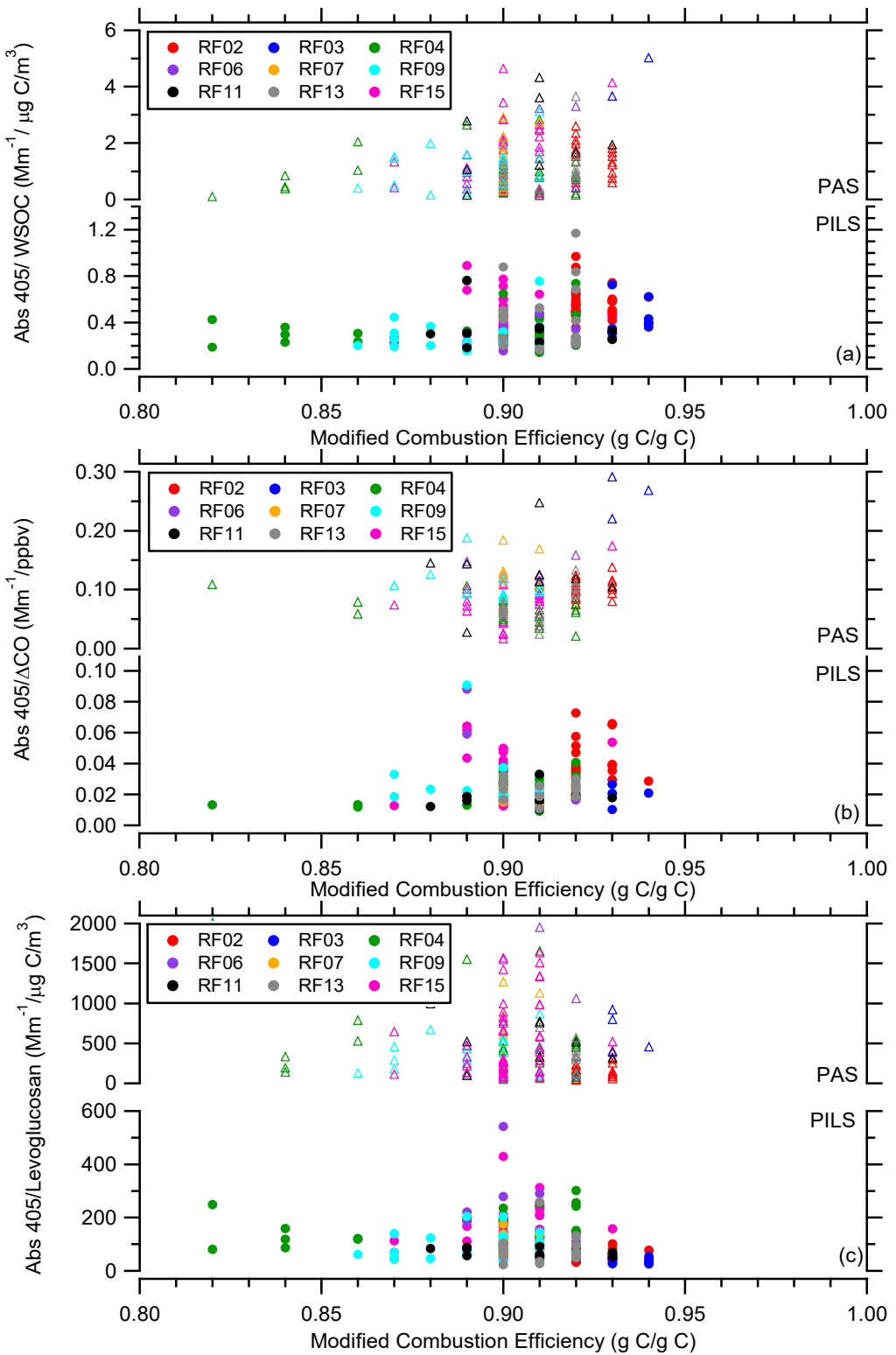
Figure 11. (a) Abs 405/WSOC, (b) Abs 405/ΔCO, and (c) Abs 405/levoglucosan as a function of modified combustion efficiency for all WE-CAN flights with the data segregated by flight. In each plot the PAS total Abs 405 BrC is on top and the PILS water-soluble Abs 405 on the bottom.

518 observed for the wildfires with higher MCE values (i.e., Flight RF02). This further supports the
519 relationship between the highest potassium concentrations and the levoglucosan vs. Abs 405
520 correlation (Figure 8) previously discussed as potassium is predominately emitted from the
521 flaming phase of a fire [*Echalar et al.*, 1995; *Lee et al.*, 2010; *Ward et al.*, 1991].
522
523 **4. Summary**
524   A PILS-LWCC-TOC and PAS were deployed on the NSF/NCAR C-130 research aircraft
525 during WE-CAN to examine aerosol absorption in wildfire smoke in the western U.S. This was
526 the first deployment of the PILS-LWCC-TOC on a research aircraft. The PILS allowed for a 16
527 s integrated measurement of the water-soluble BrC absorption and 4 s integrated measurement of
528 WSOC. The data from the PILS and PAS were combined to investigate the water-soluble vs.
529 total BrC absorption at 405 nm in the 20 wildfires sampled during WE-CAN. We show the
530 following:
531
532   1. WSOC, PILS water-soluble Abs 405, and PAS total Abs 405 BrC tracked each other in
533   and out of the smoke plumes. BrC absorption was correlated with CO (R^2 value for PAS
534   = 0.76 and PILS = 0.55) and WSOC (R^2 value for PAS = 0.42 and PILS = 0.60) during
535   the entire study, illustrating the importance of biomass burning as a source of BrC
536   absorption. A similar pattern was observed for levoglucosan, but with two data branches.
537   Levoglucosan and BrC absorption were correlated (R^2 values for PAS = 0.60 and PILS =
538   0.76) in the first data branch and this subset of data was also characterized by the highest
539   observed water-soluble potassium concentrations (> 0.5 μg/m^3). This suggests there may
540   be a relationship between levoglucosan and water-soluble potassium in wildfire
541   emissions that has not generally been observed in other types of burning.
542
543   2. Using the calculated UHSAS mass, the PILS water-soluble Abs 405 can be corrected to
544   also account for the non-water-soluble fraction of the aerosol. The corrected PILS water-
545   soluble Abs 405 showed good closure with the PAS total Abs 405 BrC, but with a factor
546   of ~1.5 to 2 difference. This difference can be explained by particle vs. bulk solution
547   absorption measured by the PAS vs. PILS, respectively, as shown by Mie Theory
548   calculations. During WE-CAN, ~45% of the BrC absorption at 405 nm was due to
549   water-soluble species.
550
551   3. The ratio of water-soluble Abs 405 to WSOC, ΔCO, or levoglucosan showed no clear
552   dependence on fire dynamics or the time since emission up to 9 h. The total Abs 405
553   BrC did show a slight decrease in the first 2 h, suggesting a need to further explore near
554   source evolution.
555
556
557
558
559
560
561
562
563

Data Availability

The WE-CAN data is provided by NCAR/EOL under sponsorship of the National Science Foundation and is available at http://data.eol.ucar.edu/master_lists/generated/we-can/. The DOI for each data set used in this work are:

PILS1: https://doi.org/10.26023/9H07-MD9K-430D and https://doi.org/10.26023/CRHY-NDT9-C30V
PILS2: https://doi.org/10.26023/7TAN-TZMD-680Y
PAS: https://doi.org/10.26023/K8P0-X4T3-TN06
UHSAS: https://doi.org/10.26023/BZ4F-EAC4-290W
CO: https://doi.org/10.26023/NNYM-Z18J-PX0Q
Meteorological Data and Coordinates: https://doi.org/10.26023/G766-BS71-9V03

Author Contributions

APS, SMM, DWT, EVF, JLC designed the project. APS wrote the paper. APS, RPP, YS, SMM, DWT, TC, JL, and EVF collected and analyzed data. All authors reviewed and provided comments for the paper.

Conflict of Interest

The authors declare that they have no conflict of interest.

Acknowledgements

We wish to thank RAF personnel for their many contributions supporting the field deployment. We also thank R.J. Weber for generously providing some of the parts used in the PILS racks.

Financial Support

This work was supported by the National Science Foundation under AGS-1650786.

References

Andreae, M.O. and A. Gelencsér, Black carbon or brown carbon? The nature of light-absorbing carbonaceous aerosols, *Atmos. Chem. Phys., 6*, 3131-3148, doi:10.5194/acp-6-3131-2006, 2006.

Arnott, W.P., H. Moosmüller, C.F. Rogers, T. Jin, and R. Bruch, Photoacoustic spectrometer for measuring light absorption by aerosol: instrument description, *Atmos. Environ., 33*, 2845-2852, 1999.

Chakrabarty, R.K., H. Moosmüller, L.-W. A. Chen, K. Lewis, W.P. Arnott, C. Mazzoleni, M.K. Dubey, C.E. Wold, W.M. Hao, and S.M. Kreidenweis, Brown carbon in tar balls from smoldering biomass combustion, *Atmos. Chem. Phys., 10*, 6363-6370, doi:10.5194/acp-10-6363-2010, 2010.

Craig, L., A. Moharreri, D. C. Rogers, B. Anderson, and S. Dhaniyala, Aircraft-Based Aerosol Sampling in Clouds: Performance Characterization of Flow-Restriction Aerosol Inlets, *Journal of Atmospheric and Oceanic Technology*, *31*, 2512-2521, doi:10.1175/jtech-d-14-00022.1, 2014.

Craig, L., A. Moharreri, A. Schanot, D. C. Rogers, B. Anderson, and S. Dhaniyala, Characterizations of Cloud Droplet Shatter Artifacts in Two Airborne Aerosol Inlets, *Aerosol Sci. Tech.*, *47*, 662-671, doi:10.1080/02786826.2013.780648, 2013a.

Craig, L., A. Schanot, A. Moharreri, D. C. Rogers, and S. Dhaniyala, Design and Sampling Characteristics of a New Airborne Aerosol Inlet for Aerosol Measurements in Clouds, *Journal of Atmospheric and Oceanic Technology*, *30*, 1123-1135, doi:10.1175/jtech-d-12-00168.1, 2013b.

Desyaterik, Y., Y. Sun, X. Shen, T. Lee, X. Wang, T. Wang, and J.L. Collett Jr., Speciation of "brown" carbon in cloud water impacted by agricultural biomass burning in eastern China, *J. Geophys. Res., 118*, 7389-7399, doi:10.1022/jgrd.50561, 2013.

Di Lorenzo, R.A., B.K. Place, T.C VandenBoer, and C.J. Young, Composition of Size-Resolved Aged Boreal Fire Aerosols: Brown Carbon, Biomass Burning Tracers, and Reduced Nitrogen, *ACS Earth Space Chem., 2*, 278-285, doi:10.1021/acsearthspacechem.7b00137, 2018.

Di Lorenzo, R.A., R.A. Washenfelder, A.R. Attwood, H. Guo, L. Xu, N.L. Ng, R.J. Weber, K. Baumann, E. Edgerton, and C.J. Young, Molecular-Size-Separated Brown Carbon Absorption for Biomass-Burning Aerosol at Multiple Field Sites, *Environ. Sci. Technol., 51*, 3128-3137, doi:10.1021/acs.est.6b06160, 2017.

Duarte, R.M.B.O., C.A. Pio, and A.C. Duarte, Spectroscopic study of the water-soluble organic matter isolated from atmospheric aerosols collected under different atmospheric conditions, *Analytica Chimica Acta, 530*, 7-14, 2005.

656   Duarte, R.M.B.O., M. Piñeiro-Iglesias, P. López-Mahía, S. Muniategui-Lorenzo, J. Moreda-
657   Piñeiro, A.M.S. Silva, and A.C. Duarte, Comparative study of atmospheric water-soluble
658   organic aerosols composition in contrasting suburban environments in the Iberian
659   Peninsula Coast, *Science of the Total Environment, 648*, 430-441, 2019.
660
661   Eatough, D.J., A. Wadsworth, D.A. Eatough, J.W. Crawford, L.D. Hansen, and E.A. Lewis, A
662   multiple system, multi-channel diffusion denuder sampler for the determination of fine-
663   particulate organic material in the atmosphere, *Atmos. Environ., 27A*, 1213-1219, 1993.
664
665   Echalar, F., A. Gaudichet, H. Cachier, and P. Artaxo, Aerosol emissions by tropical forest and
666   savanna biomass burning: Characteristic trace elements and fluxes, *Geophys. Res. Lett.,*
667   *22*, 3039-3042, 1995.
668
669   Feng, Y., V. Ramanathan, and V.R. Kotamarthi, Brown carbon: a significant atmospheric
670   absorber of solar radiation?, *Atmos. Chem. Phys., 13*, 8607-8621, doi:10.5194/acp-13-
671   8607-2013, 2013.
672
673   Forrister, H., J. Liu, E. Scheuer, J. Dibb, L. Ziemba, K.L. Thornhill, B. Anderson, G. Diskin,
674   A.E. Perring, J.P. Schwarz, P. Campuzano-Jost, D.A. Day, B.B. Palm, J.L. Jimenez, A.
675   Nenes, and R.J. Weber, Evolution of brown carbon in wildfire plumes, *Geophys. Res.*
676   *Lett., 42*, 4623-4630, doi:10.1002/2015GL063897, 2015.
677
678   Foster, K., R. Pokhrel, M. Burkhart, and S. Murphy, A novel approach to calibrating a
679   photoacoustic absorption spectrometer using polydisperse absorbing aerosol, *Atmos.*
680   *Meas. Tech., 12*, 3351-3363, doi:10.5194/amt-12-3351-2019, 2019.
681
682   Gerbig, C., S. Schmitgen, D. Kley, A. Volz-Thomas, K. Dewey, and D. Haaks, An improved
683   fast-response vacuum-UV resonance fluorescence CO instrument, *J. Geophys. Res., 104*,
684   1699-1704, 1999.
685
686   Hecobian, A., X. Zhang, M. Zheng, N.H. Frank, E.S. Edgerton, and R.J. Weber, Water-soluble
687   organic aerosol material and the light-absorption characteristics of aqueous extracts
688   measured over the Southeastern United States, *Atmos. Chem. Phys., 10*, 5965-5977,
689   doi:10.5194/acp-10-5965-2010, 2010.
690
691   Hems, R.F. and J.P.D. Abbatt, Aqueous Phase Photo-oxidation of Brown Carbon Nitrophenols:
692   Reaction Kinetics, Mechanism, and Evolution of Light Absorption, *ACS Earth Space*
693   *Chem., 2*, 225-234, doi:10.1021/acsearthspacechem.7b00123, 2018.
694
695   Hoffer, A., A. Gelencsér, P. Guyon, G. Kiss, O. Schmid, G.P. Frank, P. Artaxo, and M.O.
696   Andreae, Optical properties of humic-like substance (HULIS) in biomass-burning
697   aerosols, *Atmos. Chem. Phys., 6*, 3563-3570, doi:10.5194/acp-6-3563-2006, 2006.
698
699   Jacobson, M.C., H.-C. Hansson, K.J. Noone, and R.J. Charlson, Organic atmospheric aerosols:
700   Review and state of the science, *Rev. Geophys., 38*, 267-294, 2000.
701

702   Jo, D.S., R.J. Park, S. Lee, S.-W. Kim, and X. Zhang, A global simulation of brown carbon:
703   implications for photochemistry and direct radiative effect, *Atmos. Chem. Phys., 16*,
704   3413-3432, doi:10.5194/acp-16-3413-2016, 2016.
705
706   Kanakidou, M., et al., Organic aerosol and global climate modelling: a review, *Atmos. Chem.*
707   *Phys., 5*, 1053-1123, doi:10.5194/acp-5-1053-2005, 2005.
708
709   Kirchstetter, T.W. and T.L. Thatcher, Contribution of organic carbon to wood smoke particulate
710   matter absorption of solar radiation, *Atmos. Chem. Phys., 12*, 6067-6072,
711   doi:10.5194/acp-12-6067-2012, 2012.
712
713   Kirchstetter, T.W., T. Novakov, and P.V. Hobbs, Evidence that the spectral dependence of light
714   absorption by aerosols is affected by organic carbon, *J. Geophys. Res., 109*, D21208,
715   doi:10.1029/2004JD004999, 2004.
716
717   Lack, D.A. and J.M. Langridge, On the attribution of black and brown carbon light absorption
718   using the Ångström exponent, *Atmos. Chem. Phys., 13*, 10535-10543, doi:10.5194/acp-
719   13-10535-2013, 2013.
720
721   Lack, D.A., J.M. Langridge, R. Bahreini, C.A. Brock, A.M. Middlebrook, and J.P. Schwarz,
722   Brown Carbon and Internal Mixing in Biomass Burning Particles, *P. Natl. Acad. Sci.,*
723   *109*, 14802-14807, doi:10.1073/pnas.1206575109, 2012.
724
725   Langridge, J.M., M.S. Richardson, D.A. Lack, C.A. Brock, and D.M. Murphy, Limitations of the
726   Photoacoustic Technique for Aerosol Absorption Measurement at High Relative
727   Humidity, *Aerosol Sci. Technol., 47*, 1163-1173, doi:10.1080/02786826.2013.827324,
728   2013.
729
730   Lee, T., A.P. Sullivan, L. Mack, J.L. Jimenez, S.M. Kreidenweis, T.B. Onasch, D.R. Worsnop,
731   W. Malm, C.E. Wold, W.M. Hao, and J.L. Collett, Jr., Chemical smoke marker emissions
732   during flaming and smoldering phases of laboratory open burning of wildland fuels,
733   *Aerosol Res. Lett., 44*, i-v, 2010.
734
735   Lee, A.K.Y., M.D. Willis, R.M. Healy, J.M. Wang, C.-H. Jeong, J.C. Wenger, G.J. Evans, and
736   J.P.D. Abbatt, Single-particle characterization of biomass burning organic aerosol
737   (BBOA): evidence for non-uniform mixing of high molecular weight organics and
738   potassium, *Atmos. Chem. Phys., 16*, 5561–5572, doi:10.5194/acp-16-5561-2016, 2016.
739
740   Limbeck, A., M. Kulmala, and H. Puxbaum, Secondary organic aerosol formation in the
741   atmosphere via heterogeneous reaction of gaseous isoprene on acidic particles, *Geophys.*
742   *Res. Lett, 30*(19), 1996, doi: 10.1029/2003GL017738, 2003.
743
744   Liu, J., M. Bergin, H. Guo, L. King, N. Kotra, E. Edgerton, and R.J. Weber, Size-resolved
745   measurements of brown carbon in water and methanol extracts and estimates of their
746   contribution to ambient fine-particle light absorption, *Atmos. Chem. Phys., 13*, 12389-
747   12404, doi:10.5194/acp-13-12389-2013, 2013.

748

749 Liu, J., E. Scheuer, J. Dibb, G.S. Diskin, L.D. Ziemba, K.L. Thornhill, B.E. Anderson, A.
750   Wisthaler, T. Mikoviny, J.J. Devi, M. Bergin, A.E. Perring, M.Z. Markovic, J.P.
751   Schwarz, P. Campuzano-Jost, D.A. Day, J.L. Jimenez, and R.J. Weber, Brown carbon
752   aerosol in the North American continental troposphere: sources, abundances, and
753   radiative forcing, *Atmos. Chem. Phys., 15*, 7841-7858, doi:10.5194/acp-15-7841-2015,
754   2015.

755

756 Liu, J., E. Scheuer, J. Dibb, L.D. Ziemba, K.L. Thornhill, B.E. Anderson, A. Wisthaler, T.
757   Mikoviny, J.J. Devi, M. Bergin, and R.J. Weber, Brown carbon in the continental
758   troposphere, *Geophys. Res. Lett., 41*, 2191-2195, doi:10.1002/2013GL058976, 2014.

759

760 Lukács, H., A. Gelencsér, S. Hammer, H. Puxbaum, C. Pio, M. Legrand, A. Kasper-Giebl, M.
761   Handler, A. Limbeck, D. Simspon, S. Preunkert, Seasonal trends and possible sources of
762   brown carbon based on 2-year aerosol measurements at six sites in Europe, *J. Geophys.*
763   *Res., 112*, D23S18, doi:10.1029/2006JD008151, 2007.

764

765 Marple, V.A., K.L. Rubow, and S.M. Behm, A microorifice uniform deposit impactor (MOUDI):
766   description, calibration, and use, *Aerosol Sci. Technol., 14*, 434-446, 1991.

767

768 Moharreri, A., L. Craig, P. Dubey, D. C. Rogers, and S. Dhaniyala, Aircraft testing of the new
769   Blunt-body Aerosol Sampler (BASE), *Atmos. Meas. Tech.*, *7*, 3085-3093,
770   doi:10.5194/amt-7-3085-2014, 2014.

771

772 Mohr, C., F.D. Lopez-Hilfiker, P. Zotter. A.S.H. Prévôt, L. Xu, N.L. Ng, S.C. Herndon, L.R.
773   Williams, J.P. Franklin, M.S. Zahniser, D.R. Worsnop, W.B. Knighton, A.C. Aiken, K.J.
774   Gorkowski, M.K. Dubey, J.D. Allan, and J.A. Thornton, Contribution of Nitrated Phenols
775   to Wood Burning Brown Carbon Light Absoprtion in Detling, United Kingdom during
776   Winter Time, *Environ. Sci. Technol., 47*, 6316-6324, 2013.

777

778 Moosmüller, H., R.K. Chakrabarty, W.P. Arnott, Aerosol light absorption and its measurement:
779   A review, *J. Quant. Spectrosc. Radiat. Transfer, 110*, 844-878,
780   doi:10.1016/j.jqsrt.2009.02.035, 2009.

781

782 Orsini, D.A., Y. Ma, A. Sullivan, B. Sierau, K. Baumann, and R.J. Weber, Refinements to the
783   particle-into-liquid sampler (PILS) for ground and airborne measurements of water-
784   soluble aerosol composition, *Atmos. Environ., 37*, 1243-1259, 2003.

785

786 Palm, B.B., Q. Peng, C.D. Fredrickson, B.H. Lee, L.A. Garofalo, M.A. Pothier, S.M.
787   Kreidenweis, D.K. Farmer, R.P. Pokhrel, Y. Shen, S.M. Murphy, W. Permar, L. Hu, T.L.
788   Campos, S.R. Hall, K. Ullmann, X. Zhang, F. Flocke, E.V. Fischer, and J.A. Thornton,
789   Quantification of organic aerosol and brown carbon evolution in fresh wildfire plumes, *P.*
790   *Natl. Acad. Sci., 117*, 29469–29477, doi:10.1073/pnas.2012218117, 2020.

791

792 Pokhrel, R.P., E.R. Beamesderfer, N.L. Wagner, J.M. Langridge, D.A. Lack, T. Jayarathne, E.A.
793   Stone, C.E. Stockwell, R.J. Yokelson, and S.M. Murphy, Relative importance of black

794   carbon, brown carbon, and absorption enhancement from clear coatings in biomass
795   burning emissions, *Atmos. Chem. Phys., 17*, 5063-5078, doi:10.5194/acp-17-5063-2017,
796   2017.
797
798 Saleh, R., C.J. Hennigan, G.R. McMeeking, W.K. Chuang, E.S. Robinson, H. Coe, N.M.
799   Donahue, and A.L. Robinson, Absorptivity of brown carbon in fresh and photo-
800   chemically aged biomass-burning emissions, *Atmos. Chem. Phys., 13*, 7683-7693,
801   doi:10.5194/acp-13-7683-2013, 2013.
802
803 Sareen, N., A.N. Schwier, E.L. Shapiro, D. Mitroo, and V.F. McNeill, Secondary organic
804   material formed by methylglyoxal in aqueous aerosol mimics, *Atmos. Chem. Phys., 10*,
805   997-1016, doi:10.5194/acp-10-977-2010, 2010.
806
807 Saxena, P. and L.M. Hildemann, Water-soluble organics in atmospheric particles: A critical
808   review of the literature and applications of thermodynamics to identify candidate
809   compounds, *J. Atmos. Chem., 24*, 57-109, 1996.
810
811 Schauer, J.J., M.J. Kleeman, G.R. Cass, and B.R.T. Simoneit, Measurement of Emissions from
812   Air Pollution Sources. 3. C_1-C_{29} Organic Compounds from Fireplace Combustion of
813   Wood, *Environ. Sci. Technol., 35*, 1716-1728, 2001.
814
815 Simoneit, B.R.T., J.J. Schauer, C.G. Nolte, D.R. Oros, V.O. Elias, M.P. Fraser, W.F. Rogge, and
816   G.R. Cass, Levoglucosan, a tracer for cellulose in biomass burning and atmospheric
817   particles, *Atmos. Environ., 33*, 173-182, 1999.
818
819 Sorooshian, A., F.J. Brechtel, Y. Ma, R.J. Weber, A. Corless, R.C. Flagan, and J.H. Seinfeld,
820   Modeling and Characterization of a Particle-into-Liquid Sampler (PILS), *Aerosol Sci.*
821   *Technol., 40*, 396-409, 2006.
822
823 Sullivan, A.P., H. Guo, J.C. Schroder, P. Campuzano-Jost, J.L. Jimenez, T. Campos, V. Shah, L.
824   Jaeglé, B.H. Lee*, F.D. Lopez-Hilfiker, J.A. Thornton, S.S. Brown, and R.J. Weber,
825   Biomass Burning Markers and Residential Burning in the WINTER Aircraft Campaign,
826   *J. Geophys. Res., 124*, doi:10.1029/2017JD028153, 2019.
827
828 Sullivan, A.P., N. Frank, D.M. Kenski, and J.L. Collett Jr., Application of High-Performance
829   Anion-Exchange Chromatography – Pulsed Amperometric Detection for Measuring
830   Carbohydrates in Routine Daily Filter Samples Collected by a National Network: 2.
831   Examination of Sugar Alcohols/Polyols, Sugars, and Anhydrosugars in the Upper
832   Midwest, *J. Geophys. Res., 116*, D08303, doi:10.1029/2010JD014169, 2011b.
833
834 Sullivan, A.P., N. Frank, G. Onstad, C.D. Simpson, and J.L. Collett, Jr., Application of High-
835   Performance Anion-Exchange Chromatography – Pulsed Amperometric Detection for
836   Measuring Carbohydrates in Routine Daily Filter Samples Collected by a National
837   Network: 1. Determination of the Impact of Biomass Burning in the Upper Midwest, *J.*
838   *Geophys. Res., 116*, D08302, doi:10.1029/2010JD014166, 2011a.
839

840 Sullivan, A.P., A.A. May, T. Lee, G.R. McMeeking, S.M. Kreidenweis, S.K. Akagi, R.J.
841   Yokelson, S.P. Urbanski, and J.L. Collett, Jr., Airborne-Based Source Smoke Marker
842   Ratios from Prescribed Burning, *Atmos. Chem. Phys., 14*, 10535-10545, doi:10.5194/acp-
843   14-10535-2014, 2014.
844
845 Sumlin, B.J., A. Pandey, M.J. Walker, R.S. Pattison, B.J. Williams, and R.K. Chakrabarty,
846   Atmospheric Photooxidation Diminishes Light Absorption by Primary Brown Carbon
847   Aerosol from Biomass Burning, *Environ. Sci. Technol. Lett., 4*, 540-545,
848   doi:10.1021/acs/estlett.7b00393, 2017.
849
850 Updyke, K.M., T.B. Nguyen, and S.A. Nizkorodov, Formation of brown carbon via reactions of
851   ammonia with secondary organic aerosols from biogenic and anthropogenic precursors,
852   *Atmos. Environ., 63*, 22-31, 2012.
853
854 Verma, V., Y. Wang, R. El-Afifi, T. Fang, J. Rowland, A.G. Russell, and R.J. Weber,
855   Fractionating ambient humic-like substances (HULIS) for their reactive oxygen species
856   activity – Assessing the importance of quinones and atmospheric aging, *Atmos. Environ.,
857   120*, 351-359, 2015.
858
859 Washenfelder, R.A., L. Azzarello, K. Ball, S.S. Brown, Z.C.J. Decker, A. Franchin, C.D.
860   Fredrickson, K. Hayden, C.D. Holmes, A.M. Middlebrook, B.B. Palm, R.B. Pierce, D.J.
861   Price, J.M. Roberts, M.A. Robinson, J.A. Thornton, C.C. Womack, and C.J. Young,
862   Complexity in the Evolution, Composition, and Spectroscopy of Brown Carbon in
863   Aircraft Measurements of Wildfire Plumes, *Geophys. Res. Lett., 49*, e2022GL098951,
864   doi:10.1029/2022GL098951, 2022.
865
866 Ward, D.E. and L.F. Radke, Emission measurements from vegetation fires: a comparative
867   evaluation of methods and results, in *Fire in the environment: the ecological,
868   atmospheric, and climatic importance of vegetation fires*, edited by P.J. Crutzen and J.G.
869   Goldammer, pp. 53-76, Wiley, Chichester, England, 1993.
870
871 Ward, D.E., A.W. Setzer, Y.J. Kaufman, and R.A. Rasmussen, Characteristics of smoke
872   emissions from biomass fires of the Amazon region-BASE-A experiment, in *Global
873   Biomass Burning: Atmospheric, Climatic, and Biospheric Implications*, edited by J.S.
874   Levine, pp. 394-402, MIT Press, Cambridge, MA, 1991.
875
876 Wong, J.P.S., M. Tsagkaraki, I. Tsiodra, N. Mihalopoulos, K. Violaki, M. Kanakidou, J.
877   Sciare, A. Nenes, and R.J. Weber, Atmospheric evolution of molecular-weight-
878   separated brown carbon from biomass burning, *Atmos. Chem. Phys., 19*, 7319-7334,
879   doi:10.5194/acp-19-7319-2019, 2019.
880
881 Yttri, K.E., W. Aas, A. Bjerke, J.N. Cape, F. Cavalli, D. Ceburnis, C. Dye, L. Emblico, M.C.
882   Facchini, C. Forster, J.E. Hanssen, H.C. Hansson, S.G. Jennings, W. Maenhaut, J.P.
883   Patau, and K. Tørseth, Elemental and organic carbon in PM10: a one year
884   measurement campaign within the European Monitoring and Evaluation Programme
885   EMEP, *Atmos. Chem. Phys., 7*, 5711-5725, 2007.

886
887 Zeng, L., J. Dibb, E. Scheuer, J.M. Katich, J.P. Schwarz, I. Bourgeois, J. Peischl, T. Ryerson,
888   C. Warneke, A.E. Perring, G.S. Diskin, J.P. DiGangi, J.B. Nowak, R.H. Moore, E.B.
889   Wiggins, D. Pagonis, H. Guo, P. Campuzano-Jost, J.L. Jimenez, L. Xu, and R. J.
890   Weber, Characteristics and Evolution of Brown Carbon in Western United States
891   Wildfires, *Atmos. Chem. Phys, 22*, 8009-8036, doi:10.5194/acp-22-8009-2022, 2022.
892
893 Zeng, L., A. Zhang, Y. Wang, N.L. Wagner, J.M. Katich, J.P. Schwarz, G.P. Schill, C.
894   Brock, K.D. Froyd, D.M. Murphy, C.J. Williamson, A. Kupac, E. Scheuer, J. Dibb,
895   and R.J. Weber, Global Measurements of Brown Carbon and Estimated Direct
896   Radiative Effects, *Geophys. Res. Lett., 47*, e2020GL088747,
897   doi:10.1029/2020GL088747, 2020.
898
899 Zhang, A., Y. Wang, Y. Zhang, R.J. Weber, Y. Song, Z. Ke, and Y. Zou, Modeling the
900   global radiative effect of brown carbon: a potentially larger heating source in the
901   tropical free troposphere than black carbon, *Atmos. Chem. Phys., 20*, 1901-1920,
902   doi:10.5194/acp-20-1901-2020, 2020.
903
904 Zhang, Q., et al., Ubiquity and dominance of oxygenated species in organic aerosols in
905   anthropogenically-influenced Northern Hemisphere midlatitudes, *Geophys. Res. Lett.,*
906   *34*, L13801, doi:10.1029/GL029979, 2007.
907
908 Zhang, X., Y.-H. Lin, J.D. Surratt, and R.J. Weber, Sources, Composition and Absorption
909   Ångström Exponent of Light-absorbing Organic Components in Aerosol Extracts
910   from the Los Angeles Basin, *Environ. Sci. Technol., 47*, 3685-3693,
911   doi:10.1021/es305047b, 2013.
912
913 Zhang, X., Y.-H. Lin, J.D. Surratt, P. Zotter, A.S.H. Prévôt, and R.J. Weber, Light-absorbing
914   soluble organic aerosol in Los Angeles and Atlanta: A contrast in secondary organic
915   aerosol, *Geophys. Res. Lett., 38*, L21810, doi:10.1029/2011GL049385, 2011.
916
917 Zhang, Y., H. Forrister, J. Liu, J. Dibb, B. Anderson, J.P. Schwarz, A.E. Perring, J.L.
918   Jimenez, P. Campuzano-Jost, Y. Wang, A. Nenes, and R.J. Weber, Top-of-
919   atmosphere radiative forcing affected by brown carbon in the upper troposphere,
920   *Nature Geoscience, 10*, 486-489, doi:10.1038/NGEO2960, 2017.
921
922 Zhao, R., A.K.Y. Lee, L. Huang, X. Li., F. Yang, and J.P.D. Abbatt, Photochemical
923   processing of aqueous atmospheric brown carbon, *Atmos. Chem. Phys., 15*, 6087-
924   6100, doi:10.5194/acp-15-6087-2015, 2015.
925
926 Zhong, M. and M. Jang, Dynamic light absorption of biomass-burning organic carbon
927   photochemically aged under natural sunlight, *Atmos. Chem. Phys., 14*, 1517-1525,
928   doi:10.5194/acp-14-1517-2014, 2014.
929